ACCSCIENCE PUBLISHING

Engineering Science in Additive Manufacturing

REVIEW ARTICLE

Recent advances in thermal management via additive manufacturing

Sooyeon Ji†, Junyeol Choi†, Myounggi Hong†, Jeongwoo Lee, Yong Choi, Jiheon Kim, Jaemin Lee*, and Wonjoon Choi*

School of Mechanical Engineering, Korea University, Seongbuk-Gu, Seoul, Republic of Korea

Abstract

Additive manufacturing (AM) has emerged as a transformative approach for advancing thermal management technologies, providing unprecedented freedom in design, material customization, and the implementation of novel thermal control strategies. This review presents a comprehensive overview of recent progress in AM-enabled thermal management, with an emphasis on enhancements in conductive, convective, boiling, and radiative heat transfer. AM facilitates the fabrication of complex architectures and composite materials with tailored thermal conductivities, substantially improving heat dissipation in diverse applications, including electronics, automotive systems, aerospace structures, and building technologies. Notably, recent developments in thermal metamaterials—such as structures capable of thermal cloaking and directional heat conduction—highlight the considerable potential of AM for manipulating complex thermal fields. Furthermore, the integration of phase change materials within AM-fabricated structures offers improved energy storage capacity and efficient thermal regulation. Future research should focus on the development of advanced composite materials, the integration of artificial intelligence for design optimization, the exploration of multifunctional metamaterials, and the advancement of sustainable and scalable AM processes. Hybrid and multimaterial AM techniques are particularly promising, enabling the fabrication of complex, functionally graded structures with precisely tailored thermal and mechanical properties. Addressing critical challenges—including structural integrity, microstructural control, material scalability, cost-effective production, and environmental sustainability—will further strengthen the role of AM in thermal management. In addition, the continued incorporation of high-fidelity computational simulations and real-time monitoring into AM workflows is expected to enhance process reliability and reproducibility. Expanding the range of AM applications to encompass lightweight and optically transparent polymer-based devices could unlock new avenues for thermal management in sensitive electronic and photonic systems.

Keywords: Thermal management; Conduction heat transfer; Convection heat transfer; Boiling heat transfer; Radiative cooling; Phase change material; Thermal metamaterial

1. Introduction

Thermal management is a critical aspect of modern engineering, impacting sectors from electronics cooling to building energy efficiency. The global building sector, for

†*These authors contributed equally to this work.*

***Corresponding authors:**
Jaemin Lee
(jmlee3025@korea.ac.kr)
Wonjoon Choi
(wojchoi@korea.ac.kr)

Citation: Ji S, Choi J, Hong M, *et al*. Recent advances in thermal management via additive manufacturing. *Eng Sci Add Manuf*. 2025;1(3):025260016. doi: 10.36922/ESAM025260016

Received: June 24, 2025

Revised: July 22, 2025

Accepted: July 28, 2025

Published online: August 18, 2025

example, consumes approximately 34% of energy and contributes 37% of global CO_2 emissions; improving insulation and thermal efficiency of building materials is a high priority.[1] At the same time, electronic and automotive systems are dissipating ever-higher heat fluxes due to device miniaturization and increased power density.[2,3] Conventional passive cooling solutions (e.g., air-cooled aluminum heat sinks) are approaching performance limits as heat fluxes can exceed 50–100 W/cm^2 in advanced devices.[4] These trends drive the need for new materials and designs that can spread and remove heat more effectively while minimizing weight and volume.

Additive manufacturing (AM) refers to layer-by-layer fabrication processes capable of producing complex and intricate geometries directly from digital models.[5] This innovative technology transforms digital designs into physical objects by successively depositing material layers, offering unparalleled flexibility and precision in manufacturing. Compared to traditional subtractive manufacturing methods, which involve removing material from a solid block, AM provides unprecedented geometric freedom. This freedom enables the creation of sophisticated internal structures such as lattices, fins, and porous architectures, which are challenging or even impossible to fabricate through conventional methods. In addition, AM allows precise control over the internal geometry, enabling designers to realize intricate and optimized structures tailored for specific applications.[6] Furthermore, AM facilitates the precise and customizable placement of materials, making it possible to produce advanced composite materials and functionally graded structures.[7-9] Such tailored material distributions allow engineers to finely adjust mechanical and thermal properties to satisfy stringent performance requirements and address complex design challenges.

In thermal management applications, these capabilities of AM offer substantial improvements in performance along with unprecedented design freedom compared to traditional fabrication techniques. For example, intricate and complex internal cooling channels can be directly integrated within heat exchangers, enabling efficient coolant circulation and significantly enhancing overall heat dissipation performance.[10] Furthermore, various lattice structures can be designed and fabricated to substantially increase the available surface area for heat transfer, effectively maximizing convective heat transfer efficiency.[11] In addition, AM technology allows precise control over the selection and placement of materials, enabling the production of customized composite structures optimized for specific thermal requirements. For instance, highly thermally conductive materials such as metallic or carbon-based fillers can be selectively incorporated in regions demanding high thermal conductivity.[12,13] Similarly, regions requiring enhanced radiative cooling performance can incorporate nanomaterials or nanoscale structures exhibiting high emissivity, thereby significantly boosting the overall thermal performance of the system.[14] Another notable advantage is the ability of AM processes to unify multiple individual thermal management components into a single integrated structure.[15] Such integrated designs drastically reduce thermal interface resistances arising from joints between separate components, thereby enhancing system reliability, durability, and thermal performance. Moreover, this approach simplifies manufacturing procedures and reduces production costs. Finally, AM technologies facilitate the creation of advanced thermal metamaterials specifically engineered to precisely manipulate heat flow characteristics, including directionality and magnitude.[16,17] These thermal metamaterials can achieve functionalities previously unattainable with conventional materials, such as thermal focusing, cloaking, and directional heat conduction. Consequently, AM-driven thermal metamaterials represent an innovative class of solutions, providing entirely new possibilities for controlling and managing thermal energy. Therefore, continuous development and adoption of AM technology are expected to play a critical role in advancing future thermal management solutions.

This review provides a comprehensive overview of how AM is advancing the field of thermal management. Section 2 introduces common AM methods and heat transfer mechanisms. Section 3 discusses conductive heat transfer: Enhancing thermal conductivity via AM-fabricated composites, achieving thermal insulation with lightweight structures and phase change materials (PCMs), and designing thermal metamaterials. Section 4.1 covers convection: passive and active heat sink innovations, micro/mini-channel and triply periodic minimal surface (TPMS)-based heat exchangers, and topology-optimized cooling structures. The latter part of section 4 addresses boiling heat transfer, both pool and flow boiling, including 3D-printed surfaces and two-phase devices. Section 5 discusses radiation heat transfer and passive daytime radiative cooling. The paper concludes with an outlook on future research directions, noting that while AM enables unprecedented thermal management designs, careful consideration of material behavior and fluid dynamics is required to fully capitalize on its potential.

2. AM for thermal management applications

2.1. AM techniques

AM, widely known as 3D printing, encompasses various layer-by-layer fabrication processes enabling intricate and

customized designs, which are impossible with traditional manufacturing methods. The primary AM techniques include material extrusion (MEX), vat photopolymerization (VPP), powder bed fusion (PBF), direct energy deposition, material jetting (MJ), and sheet lamination (SHL).[18]

MEX is a widely used AM technique, involving the selective deposition of materials through an extrusion nozzle to build 3D structures layer-by-layer. Prominent examples of MEX methods include fused filament fabrication (FFF) and direct ink writing (DIW). FFF is the most common MEX method, in which thermoplastic polymer filaments are melted in a heated nozzle and extruded layer-by-layer. DIW differs from FFF by extruding viscous inks, slurries, or pastes through a nozzle using pneumatic or mechanical pressure to form intricate structures directly. In thermal management using AM, materials employed in each MEX method are typically enhanced by mixing thermally conductive substances such as metals or ceramics to improve heat dissipation performance. In the specific case of DIW, materials are often structured into aerogels to significantly enhance thermal insulation performance. Beyond the conduction heat transfer mechanism, polymer composites used in MEX have also been primarily employed to regulate the radiation heat transfer mechanism by effectively interacting with infrared (IR).

VPP methods, such as stereolithography (SLA) and digital light processing (DLP), polymerize liquid resins via ultraviolet (UV) or visible light exposure. These methods produce high-resolution, smooth surfaces and complex geometries ideal for prototypes and intricate structures. For thermal management, fillers with high thermal conductivity (e.g., carbon-based materials and ceramics) are often incorporated into polymer resins. Therefore, this method is mainly used to control the conduction heat transfer mechanism.

Laser PBF (L-PBF) includes techniques such as direct metal laser sintering (DMLS), selective laser sintering, selective laser melting (SLM), and electron beam melting. These processes use thermal energy sources, such as lasers or electron beams, to fuse powdered materials, ranging from polymers and metals to ceramics. The strengths of PBF include superior mechanical properties, dimensional accuracy, and intricate structural capabilities. Due to these strengths, particularly the ability to fabricate complex structures with metals exhibiting high thermal conductivity, PBF has found practical applications across various thermal management fields. However, challenges involve high equipment costs, residual stress management, and porosity control.[19,20] In response to these challenges, particularly in metal-based L-PBF processes, there has been growing interest in simulation-based approaches to efficiently capture and manage the complex thermodynamic behavior.[21] Due to its capability to process metal powders, this technique is predominantly applied in controlling conduction and convection heat transfer mechanisms.

Directed energy deposition (DED) employs concentrated thermal energy, typically a laser, electron beam, or plasma arc, to melt and fuse material feedstock delivered as powders or wires. DED is effective for repairing high-value parts and fabricating large components with graded compositions. Yet, it faces challenges related to precision, surface finish, and thermal distortion. This fabrication technique is mainly employed to produce components designed for use in convection heat transfer mechanisms.

MJ involves jetting droplets of photopolymer or wax onto a build platform and subsequently curing them using UV light. MJ achieves high resolution and multimaterial capability, essential for functional prototypes and detailed models. However, it is limited by relatively slow build speeds and expensive materials. This method is primarily applied to the conduction mechanism.

SHL, exemplified by laminated object manufacturing and ultrasonic AM, bonds sheets of materials—typically metal foils, paper, or plastics—via adhesive or ultrasonic welding. It is suitable for large, layered components with embedded electronics but suffers from limited structural strength and design complexity compared to other AM techniques.

Each of these AM methods has unique advantages and inherent limitations, making method selection critical depending on targeted application needs, material requirements, structural complexity, and economic considerations.

2.2. Various heat transfer mechanisms for thermal management

Effective thermal management is critical in a broad spectrum of applications, from electronic cooling to energy systems. Achieving optimal thermal regulation involves utilizing various heat transfer mechanisms—conduction, convection, boiling, and radiation, each offering distinct advantages and characteristics.

Conduction heat transfer is fundamental and occurs through direct molecular or atomic interactions, typically occurring within solid materials, liquids, or gases at rest. It relies on temperature gradients, where heat spontaneously flows from regions of higher temperature to those of lower temperature due to particle vibrations and collisions. In

solids, particularly metals, conduction is highly efficient due to free electrons facilitating rapid energy transfer. The governing law for conduction is Fourier's law, expressed as Equation I:

$$q = -k\nabla T \quad (I)$$

Where q is the local heat flux density, W/m^2; k is the thermal conductivity, W/(m·K); and ∇T is the temperature gradient, K/m. Materials with high thermal conductivity, such as metals or ceramics, are excellent thermal conductors, whereas those with low thermal conductivity, such as polymers or aerogels, are effective insulators. Enhancing conduction involves incorporating highly conductive fillers (e.g., metal/metal oxide particles, carbon nanotubes [CNT], boron nitrides [BN]) into materials to improve heat dissipation.[22,23] Conversely, minimizing conduction for insulation purposes involves porous materials or aerogels to reduce the solid conduction pathways. Conduction heat transfer is critical in applications ranging from electronics cooling to building insulation design, significantly impacting energy efficiency and thermal management effectiveness.

Convection heat transfer refers to the transport of thermal energy due to the bulk movement of fluids, including liquids and gases. Unlike conduction, which relies on molecular vibration without bulk fluid movement, convection involves fluid motion that enhances heat transfer rates significantly. Convection can be categorized into natural (free) and forced convection. Natural convection occurs due to density variations within fluids, caused by temperature gradients; warmer fluids expand, becoming less dense and rising, while cooler fluids descend. In contrast, forced convection involves external forces—such as pumps, fans, or blowers—to actively drive fluid motion, thus increasing heat transfer efficiency. Newton's law of cooling mathematically describes convection as Equation II:

$$q = hA(Ts - T_\infty) \quad (II)$$

Where q is the heat transfer rate, W/m^2; h is the convective heat transfer coefficient, W/(m^2·K); A the surface area, m^2; T_s is the temperature of the surface, K; and T_∞ is the temperature of the fluid, K. Convection is pivotal in engineering applications such as heat exchangers, electronics cooling systems, HVAC design, and thermal management of engines. Optimizing convective heat transfer involves techniques such as employing fins, microchannels, or enhancing fluid turbulence, which significantly impact overall system efficiency and reliability.

Boiling heat transfer is a highly efficient thermal energy transport mechanism involving phase change from liquid to vapor. When a heated surface exceeds the liquid's saturation temperature, boiling initiates, forming vapor bubbles. Boiling is classified primarily into two types: Pool boiling and flow boiling. Pool boiling occurs in stagnant fluids, whereas flow boiling occurs in fluids forced over heated surfaces. The boiling curve identifies different boiling regimes—natural convection boiling, nucleate boiling, transition boiling, and film boiling—each with unique heat transfer characteristics (Figure 1A).[24] Nucleate boiling is especially effective, characterized by rapid bubble nucleation, growth, and departure, providing high heat-transfer coefficients (HTC) due to vigorous mixing near the heated surface. Critical heat flux (CHF) marks the transition to film boiling, where a vapor film insulates the surface, dramatically decreasing heat transfer efficiency. Enhancing boiling performance often involves surface modification techniques such as microstructures, porous coatings, or AM to increase nucleation sites, promoting efficient bubble dynamics.[25,26]

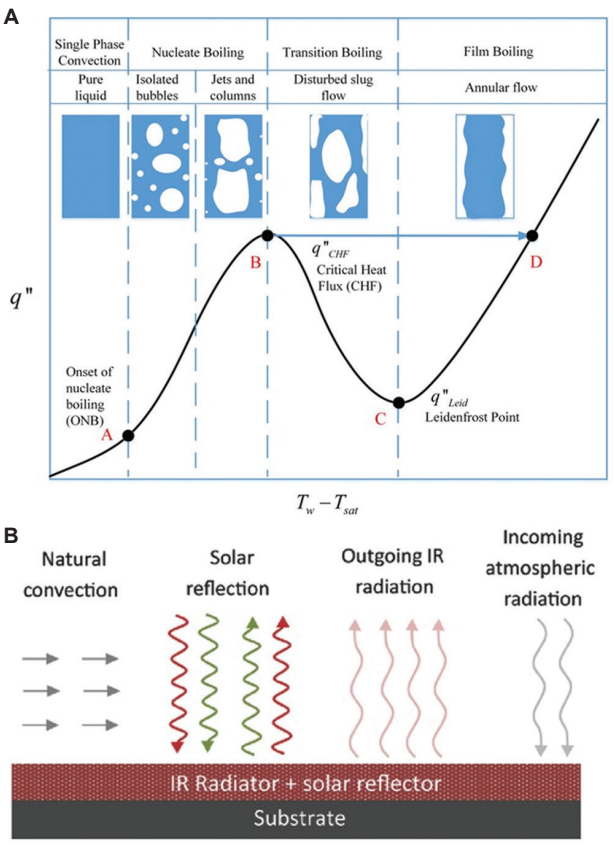

Figure 1. Examples of heat transfer mechanisms. (A) Boiling heat transfer.[24] Representative wall superheat and heat flux relation in the boiling phenomenon and bubble mechanism. (B) Radiative cooling.[27] Non-radiative heat transfer (e.g., natural convection), reflected or absorbed energy to the material from solar irradiation, the outgoing IR radiative energy emitted by the material, and incoming radiative heat to the material from the atmosphere.

Thermal transport devices leveraging liquid-to-vapor phase transitions include heat pipes and vapor chambers. Within a sealed, near-vacuum environment, the working fluid evaporates at the heated region (evaporator) and condenses at the cooler region (condenser). The condensed fluid then returns to the evaporator by capillary action, effectively transferring heat from the evaporator to the condenser. Applications of boiling heat transfer and phase-change devices span high-power electronics cooling, nuclear reactors, refrigeration systems, and chemical processing, highlighting their critical roles in advanced thermal management solutions.

Radiation heat transfer provides unique advantages, particularly in thermal management applications where conductive or convective pathways are limited. Radiative cooling technologies utilize engineered coatings and films designed with selective emissivity characteristics to exploit atmospheric transparency windows, effectively radiating heat into space without external energy input (Figure 1B).[27] Recent advancements include selective emitters and specialized radiative cooling coatings capable of achieving sub-ambient temperatures even under direct sunlight, highlighting their efficiency as passive cooling solutions. Due to these benefits, radiation cooling technologies are increasingly employed in sustainable thermal management applications such as building roofs, solar panels, electronics cooling, and space cooling systems. As a passive, energy-free method, radiation cooling represents an attractive and sustainable approach to energy conservation and thermal regulation.

In conclusion, understanding and exploiting these various heat transfer mechanisms through advanced material engineering and manufacturing processes like AM offer promising pathways to achieving superior thermal management solutions. Each mechanism, individually or in combination, can be optimized to meet specific thermal management challenges across diverse application domains.

3. Conduction heat transfer for thermal management using AM

3.1. Thermal conductivity enhancement through AM

Conductive heat transfer is mainly used to fabricate fundamental structures that can reinforce the performance of other heat transfer mechanisms. In this section, we focus on how AM technologies utilizing metallic, non-metallic, or hybrid materials can be strategically employed to tailor thermal conductivity. Specifically, we highlight approaches to increase thermal conductivity for efficient heat dissipation, decrease it for thermal insulation, and precisely control heat flow for the development of thermal metamaterials designed to direct or block heat as required.

In metal-based AM, desired geometries are fabricated by melting and solidifying metal particles using energy sources such as lasers or electron beams. In this process, both the particle size and composition of metal particles critically influence the resulting grain structure and thermal conductivity. A representative study used 316L stainless steel powder particles to control microstructure via electron beam PBF and laser-DED processes.[12] Unlike the columnar coarse crystals commonly found in traditional PBF processes, this work demonstrated that coarse particles in the powder bed undergo uneven melting, acting as seeds to induce fine spherical grains with high strength and ductility. Similarly, analysis of CoFeNi and CoCrFeNi high-entropy alloy systems revealed that lower thermal conductivity correlates with slower laser melting/cooling rates, influencing solidification patterns such as wider/longer remelted columnar grains.[28] As the grain size decreases, the density of grain boundaries increases, which enhances electron scattering at the interfaces and results in reduced thermal conductivity. Therefore, in metal-based AM processes, controlling grain size during fabrication is essential for improving thermal conductivity.

In addition, localized high-temperature melting and repeated powder reuse result in surface oxidation of metal powders and melt pools, forming oxide inclusions. These oxide layers and inclusions further decrease thermal conductivity within the metallic structure and increase interfacial thermal resistance, hindering heat transfer in the melt pool and deteriorating interlayer bonding quality. The presence of oxide films also decreases molten metal wettability, causing incomplete fusion between layers and interface defects such as micro-porosity, thus compromising structural reliability. Such oxidation effects and elevated interfacial thermal resistance adversely affect thermal and mechanical properties in practical applications, increasing residual stresses and complicating subsequent welding processes, ultimately diminishing component performance and reliability. Therefore, precise grain size control and careful oxidation management during fabrication are essential for optimizing thermal conductivity and structural integrity in metal-based AM processes.

To enhance thermal conductivity, the grain size can be increased by controlling the laser scan speed during the metal AM process. In the case of Cu-Al-Ni-Mn shape-memory alloys, the high thermal conductivity of the Cu and the shape-memory effect are advantageous. It was observed that increasing the scan speed leads to a reduction in martensite size, whereas lower scan speeds

result in less grain refinement and consequently higher thermal conductivity (Figure 2A and Table 1).[29] In another study, a CuNi2SiCr alloy fabricated via L-PBF exhibited a low thermal conductivity of approximately 70 W/(m·K) (at room temperature) due to increased free electron scattering from the supersaturated matrix containing Ni, Si, and Cr; however, after a heat treatment at 500°C for 3 h, nanoscale precipitates containing Ni, Si, and Cr formed with the matrix, reducing the concentration of alloying elements in solid solution. This microstructural change increased the electron mean free path from 5.6 nm to 13.4 nm—an elevation of about 2.4 times—resulting in a significant improvement in thermal conductivity reaching up to 180 W/(m·K) in the heat-treated samples (at room temperature).[30] In addition, incorporating graphene into aluminum using L-PBF achieved a 25.5 × 10-^{6}/°C lower coefficient of thermal expansion and approximately 10% higher thermal conductivity (140–180 W/m·K at 150–350°C) compared to conventional AlSi12 alloys.[13]

Polymer-based composites typically exhibit lower thermal conductivity compared to metals, but their excellent formability, low manufacturing costs, and low density make them particularly attractive for electric vehicles and aerospace mobility applications. Therefore, overcoming the limitation of low thermal conductivity in these polymer-based composites can enable broader substitution for metallic structures, potentially enhancing fuel efficiency of mobility platforms and reducing manufacturing costs associated with complex-shaped components. To address this, various studies have investigated enhancing thermal

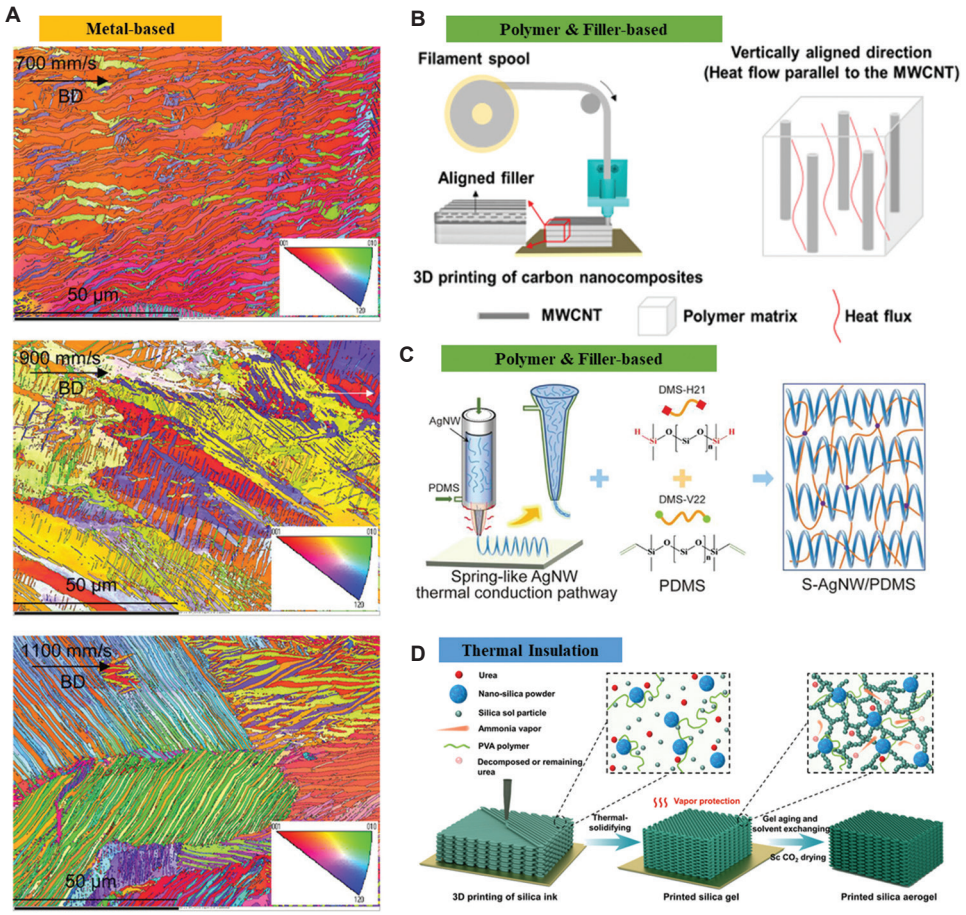

Figure 2. Thermal conductivity control using additive manufacturing. Metal-based thermal conductivity enhancement materials: (A) L-PBF of Cu–Al–Ni–Mn shape-memory alloy for the application of active heat sinks.[29] Copyright © 2023 Wiley. Reproduced with permission of Wiley. Polymer and filler-based materials: (B) MWCNT-filled PLA.[32] Copyright © 2023 American Chemical Society. Reproduced with permission of the American Chemical Society. (C) Spring-like thermal conduction pathways of silver nanowire compounded with PDMS (S-AgNW/PDMS) composites.[35] The average length and diameter of AgNW nanowires are 10.7 μm and 115 nm, respectively. The outer and inner diameters of S-AgNWs are ~1.8 mm and 1.0 mm, respectively. Copyright © 2024 Wiley. Reproduced with permission of Wiley. Thermal insulation materials: (D) 3D-printed silica aerogels by directly writing temperature-induced solidifiable inks.[43] Copyright © 2021 American Chemical Society. Reproduced with permission of the American Chemical Society.
Abbreviations: AgNW: Silver nanowire; MWCNT: Multi-walled carbon nanotubes; L-PBF: Laser powder bed fusion; PDMS: Polydimethylsiloxane; PLA: Polylactic acid; PVA: Polyvinyl alcohol; S-AgNW: Silver nanowire in spring-like structure.

Table 1. Summary of thermal conductivities measurement

Materials	AM method	Geometry	Thermal conductivity (W/[m·K])	Measured region (□)	References
Thermal conductivity enhancement					
Metal-based					
$CuNi_2SiCr$ alloy	L-PBF	Heat-treated	180–240	~25–620□	30
Graphene (25 wt%)-AlSi12 alloy	L-PBF	Carbon, Al_4C_3 cluster	140–170	~150–350□	13
Cu-Al-Ni-Mn alloys	L-PBF	Of course, low-scan rate	30–50	At 300□, 380□	29
Polymer-based			Max.		
LLDPE/BN@GNPs	FFF	Direction-dependent	3.11	Room temperature	38
BNNS (30 wt%)/TPU	FFF	Direction-dependent	1.80	Room temperature	31
MWCNT (20 wt%)/PLA	FFF	Direction-dependent	0.575	35–108□	32
Hexadecane/POE/AEO/GNPs	DIW	Direction-dependent	1.276	40□	36
Pitch carbon fiber PLA	FFF	Direction-dependent	37.1	N/A	33
3D-h-BN, graphene/PLA	FFF	Direction-dependent	3.82	N/A	37
Graphene (30 wt%)-TPU	FFF	Direction-dependent	4.54	−10–50□	39
20 vol% S-AgNW/PDMS	DIW	Direction-dependent	7.63	20–100□	35
Vertical-rGO/CNT/PDMS	DIW	Direction-dependent	6.04	Room temperature	40
h-BN/POE/Polypropylene	FA-FDM	Direction-dependent	1.43	N/A	34
Thermal insulation					
Silanized CNF aerogels	DIW	Porous aerogel	0.034	N/A	44
PLA VIP	FFF	8-interlayer panel	0.0155	15–35□	47
Silica aerogel particles/polyimide aerogel	DIW	Porous aerogel	0.076	N/A	46
PLA structures	FFF	Lamellar, cylindrical, gyroid	0.099, 0.094, 0.072	Room temperature	42

Abbreviations: AEO: Alkyl ether of ethylene oxide; AM: Additive manufacturing; BN: Boron nitride; BNNS: Boron nitride nanosheet; CNF: Cellulose nanofiber; CNT: Carbon nanotube; GNP: Graphene nanoplatelet; h-BN: Hexagonal boron nitride; MWCNT: Multi-walled carbon nanotube; LLDPE: Linear low-density polyethylene; L-PBF: Laser powder bed fusion; PDMS: Polydimethylsiloxane; PLA: Polylactic acid; POE: Polyolefin elastomer; rGO: Reduced graphene oxide; S-AgNW: Silver nanowire in spring-like structure; TPU: Thermoplastic polyurethane; VIP: Vacuum insulation panel; FFF: Fused filament fabrication; FDM: Fused deposition modeling.

conductivity by introducing fillers with high intrinsic thermal conductivity, such as nanomaterials (e.g., CNT, ceramics, and metal nanowires) and plate-like materials (e.g., graphene and BN), to establish effective pathways for rapid thermal energy transfer within the polymer matrix. Moreover, AM technologies have been actively explored to fabricate polymer composite parts or structures with significantly improved thermal performance.

A representative example of using fillers to enhance thermal conductivity involves incorporating hexagonal BN nanosheets (BNNS) into thermoplastic polyurethane (TPU) via FFF printing. Melt extrusion aligns BNNS within the TPU, achieving an in-plane thermal conductivity of 1.80 W/m·K (at room temperature) at 30 wt% BNNS, 650% higher than pure TPU.[31] Another study used multi-walled CNTs (MWCNTs) in polylactic acid (PLA) filaments, obtaining a thermal conductivity of ~0.575 W/m·K (at 35–108°C)at 20 wt% MWCNT, approximately 5.87 times higher than pure PLA due to alignment from shear forces[32] (Figure 2B). Continuous carbon fibers coated with PLA were printed using FFF, achieving a thermal conductivity of 37.1 W/m·K at 9.5 vol%, emphasizing fiber continuity's role.[33] In addition, anisotropic thermal conductivity was introduced by co-injecting thermally conductive BN fluids with polymer filaments, resulting in a composite with a conductivity of 1.43 W/m·K at 60 wt% BN.[34] This technology enables the precise design of thermally conductive pathways in heat-dissipating materials by adjusting the 3D printing model and parameters, and it has potential for use in thermal management and heat dissipation systems for electronic devices.

In MEX-based AM, not only FFF but also DIW techniques can be employed to fabricate various structures utilizing polymer composites with enhanced thermal

conductivity. For example, silver nanowire (AgNW) with high thermal conductivity filler, and polydimethylsiloxane (PDMS) composites achieved a conductivity of 7.63 W/m·K (at 20–100°C) at 20 vol% AgNW, maintaining stability under deformation[35] (Figure 2C). As described in Figure 2C, AgNWs with an average length and diameter of 10.7 μm and 115 nm, respectively, are first incorporated into PDMS (DMS-H21 + DMS-V22) and then 3D-printed into a spring-like (S-AgNW) structure. Afterwards, these S-AgNWs—with outer and inner diameters of approximately 1.8 mm and 1.0 mm, respectively—are again aligned and embedded within PDMS matrices. This 3D printing process enables the AgNWs to be arranged in a highly aligned, unidirectional structure, resulting in a remarkable enhancement of thermal conductivity along the printing direction due to the formation of an anisotropic network of conductive fillers. Another DIW composite (hexadecane/polyolefin elastomer [POE]/poly[alkyl ether of ethylene oxide] [AEO]/GNPs composites), combining hexadecane, POE, AEO, and graphene nanoplatelets (GNPs), exhibited 1.24 W/m·K (at 40°C) vertical conductivity and significantly reduced temperature differences on semiconductor surfaces compared to commercial products.[36] Although DIW differs from fused deposition modeling (FDM) in that it uses ink cured after deposition, it shares the common feature of combining polymers and fillers to boost thermal conductivity.

An important point is that research on polymer and filler composites can also be applied to develop multifunctional metamaterials and hybrid materials, such as a PLA skeleton filled with BN or graphene. These composites showed up to 3.82 W/m·K thermal conductivity with BN and enhanced mechanical strengths (20.3 MPa) and electrical insulation.[37] However, when graphene was used, the composite exhibited excellent thermal and electrical conductivity as well as a tensile strength (40.6 MPa). Compared to composites with only filler, these materials showed a 2.81-fold increase in thermal conductivity and 1.83-fold (BN filler) and 3.98-fold (graphene filler) increases in mechanical strength, respectively. Similarly, adding GNPs and BN to linear low-density polyethylene (LLDPE) created composites with thermal conductivity reaching 3.11 W/m·K (at room temperature), over 8 times higher than pure LLDPE.[38]

Research in polymer-filler composites also extends to energy applications. A bilayer structure using graphene-TPU films maximized anisotropic thermal conductivity, suitable for solar panels, with a sixfold through-plane conductivity difference.[39] Another example is a vertically printed reduced graphene oxide (rGO)/CNT-PDMS thermal interface material (TIM) device achieving 6.04 W/m·K (at room temperature) thermal conductivity, beneficial for thermal anomaly detection.[40] In this device, rGO/CNT was printed vertically by DIW, and the gaps were filled with PDMS to form the TIM. In addition, a topology-optimized aluminum structure infiltrated with PCM via SLM showed significant improvements in heat distribution and temperature uniformity.[41]

3.2. Thermal insulation using AM

In addition to heat dissipation, thermal insulation plays a crucial role in thermal management. Materials with superior insulation performance significantly reduce the energy consumption required to maintain optimal temperatures in buildings or refrigeration systems, thereby lowering greenhouse gas emissions and overall resource usage. Furthermore, enhancing insulation by achieving lower thermal conductivity allows comparable performance with reduced material thickness. This reduction substantially improves space efficiency in mobility applications and refrigeration equipment, facilitating more compact, lightweight, and energy-efficient designs.

To enhance thermal insulation performance, it is crucial to block or complicate the heat transfer pathways. Complex 3D structures based on unit cells are well-suited for this purpose, as they effectively disrupt heat flow and thereby improve insulation. In a study utilizing the FFF method, three structures—lamellar, gyroid, and cylindrical—were fabricated with the same volume fraction.[42] Among them, the lamellar structure exhibited the lowest thermal conductivity, demonstrating its superior insulating capability. However, despite their structural complexity, these architectures still exhibit higher thermal conductivity compared to conventional insulation materials. This limitation arises primarily because traditional insulators consist predominantly of air, known for its extremely low thermal conductivity. Consequently, there has been growing interest in methods capable of further reducing thermal conductivity by significantly increasing porosity. Recent studies have addressed this by combining DIW with freeze-drying to create aerogel structures characterized by ultra-low thermal conductivity, such as silica aerogels[43] (Figure 2D). For example, one study successfully fabricated an interpenetrating network structure of polymethylsilsesquioxane and cellulose nanofibers (CNFs) through DIW printing followed by freeze-drying, achieving an impressively low thermal conductivity of 0.034 W/m·K.[44] Similarly, another research group utilized lignocellulose nanofibrils to produce thermally insulating aerogels, highlighting the great potential of biopolymer-based aerogel structures fabricated by 3D printing techniques for advanced insulation applications.[45] In addition, a recent approach has explored the incorporation of silica aerogel particles into 3D-printed composite

aerogel structures to further enhance thermal insulation performance.[46]

Beyond aerogel-based methods, entirely different approaches combining 3D printing with thermal insulation technology have also emerged. One innovative example involves the use of FFF to fabricate polymer-based vacuum insulation panels (VIPs).[47] In this research, a 3D-printed VIP with eight solid interlayers was constructed under a vacuum pressure of approximately 10 Pa, achieving an exceptionally low thermal conductivity of 0.0155 W/m·K (at 15–35°C)—about 60% of the thermal conductivity of air (0.025 W/m·K). Likewise, thermal insulation aimed at preserving thermal energy is also an essential factor in thermal management, and many AM-based techniques have been utilized to address this aspect. For instance, methods such as lattice structure design, incorporation of low thermal conductivity aerogel particles, and fabrication of VIP panels with superior insulating performance have been employed to significantly enhance insulation performance.

3.3. Thermal metamaterial and PCM using AM

Advances in AM technologies have enabled the development of diverse thermal metamaterials that go beyond simply enhancing thermal conductivity or insulation performance. These advancements allow for precise control of heat flux and effective thermal energy storage across specific temperature ranges. Thermal metamaterials are materials engineered to exhibit unique thermal properties rarely found in nature and are used to manipulate or control heat transfer. 3D printing enables the free design and production of complex internal structures and diverse material combinations, greatly expanding the scope of research and applications for thermal metamaterials.

Active research is underway on thermal metamaterials that alter heat transfer pathways. For example, by integrating the theory of anisotropic thermal conductivity with custom MEX 3D printing technology, thermal cloaking functionality can be realized by embedding 0.3 mm copper wires into a PLA matrix.[17] This metal-polymer integration enhances the design freedom of thermal metamaterials and enables the fabrication of heat exchangers or temperature control devices with complex internal channels and structures. Furthermore, the required thermal conductivity distribution for desired thermal functions—such as heat concentration, rotation, and cloaking—can be calculated, divided into small grid units, and converted into a single STL file for 3D printing[48] (Figure 3A). For instance, after 3D-printing die steel (H13) and fixing it with PDMS, various thermal manipulation functions such as heat concentration (isotherms converging at the center), heat rotation (isotherms rotated by 45°C),and thermal cloaking (temperature distribution in the cloaked region matching the outside) can be experimentally confirmed. Through 3D printing, thermal metamaterials with complex shapes and functions can now be practically fabricated.

Meanwhile, research is also progressing to improve the mechanical properties and durability of thermal metamaterials. One example involves various additively manufactured lattice shapes, such as triangles, cubes, petals, and waves, using SLA, followed by chemical vapor infiltration to inject silicon carbide (SiC) whiskers inside the structures.[49] This process densely coats the lattice surfaces with SiC, effectively suppressing deformation and thermal expansion caused by temperature changes.

Efforts to maximize the performance of thermal metamaterials by combining various materials and structures continue, with recent attention on infiltrating liquid metals and PCMs into polymers to alter thermal conductivity, physical properties, specific heat, and electrical conductivity[50] (Figure 3B). For example, acrylonitrile butadiene styrene polymers fabricated by 3D printing can be placed in a vacuum chamber and infused with a Bi/In/Sn alloy liquid metal to create composites with high tensile strength (up to 35.41 MPa), thermal conductivity (up to 25.29 W/[m·K]), and electrical conductivity (up to 106 S/m)[51] (Figure 3C). These composites utilize solid-liquid phase change properties for high-power LED heat dissipation and temperature control, and also exhibit excellent electromagnetic shielding. This approach is also actively applied in energy storage research, combining PCMs. Over the past 5 years, various strategies have been developed to complement the intrinsic properties of PCMs.[52,53] A representative example is the DIW of inks mixing lignocellulose nanofibers, graphene oxide, and Pickering emulsion paraffin gel, followed by freeze-drying to create a structure with entangled paraffin microspheres.[54] This structure is used for solar-thermal-electric conversion and heat storage, with a 3D-printed concave solar collector heating up to 83.2°C,generating higher voltage and longer energy storage time than 2D planar collectors.

Research on PCM-based thermal energy storage via AM is progressing in various ways. For instance, lauric acid mixed with photocurable resin and printed by SLA effectively addresses PCM leakage issues, showing optimal thermal performance at 50% loading.[55] It exhibits 83.7 J/g latent heat enthalpy, 14.02 MPa tensile strength, and only about 1.31% loss after leakage testing (50°C, 60 min). Another study incorporated microencapsulated PCM (MEPCM), consisting of a paraffin mix as the core

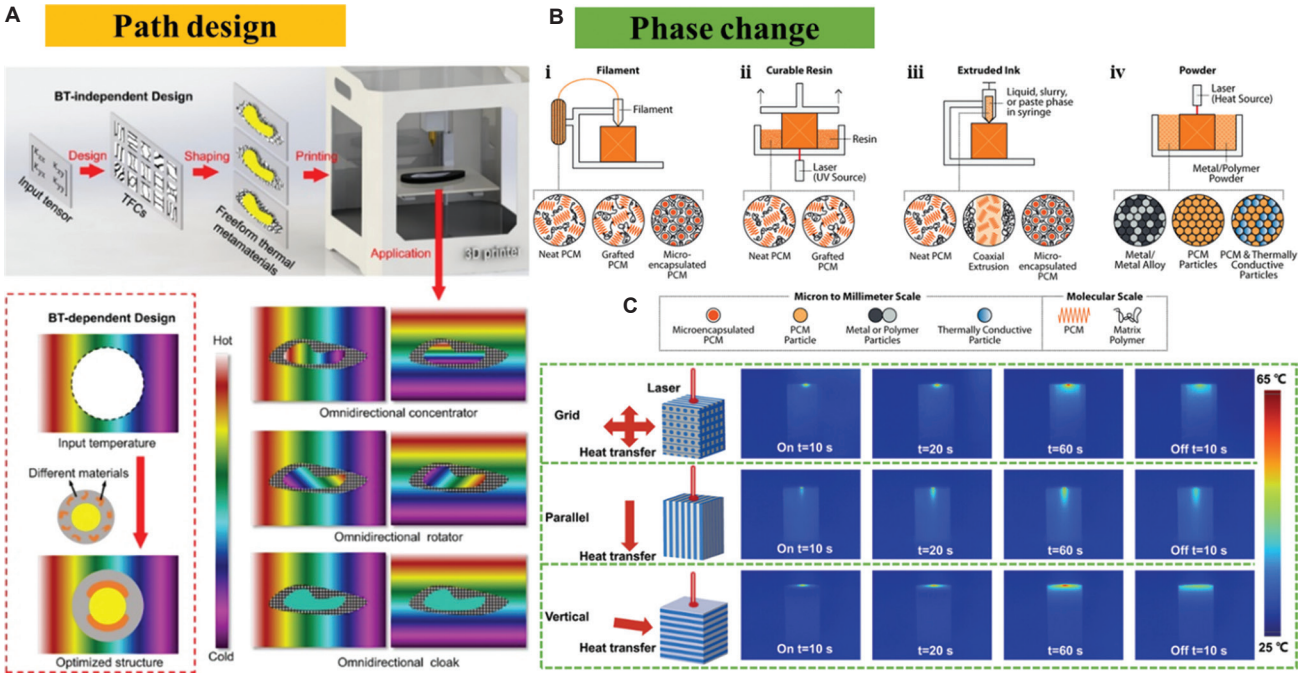

Figure 3. Thermal metamaterials using additive manufacturing. Thermal conduction path design: (A) Topological functional cells.[48] (B) Various approaches for incorporating phase change materials into material matrices: (i) fused filament fabrication or fused deposition modeling; (ii) stereolithography; (iii) direct ink writing; (iv) selective laser sintering or selective laser melting.[50] Metamaterials using phase change mechanism: (C) volume-metallization 3D-printed polymer composite.[51] Copyright © 2024 Wiley. Reproduced with permission of Wiley.

and melamine-formaldehyde as the shell in 15–30 μm spheres, into SLA resin, producing composites that absorb and release heat with temperature changes, significantly improving thermal stability and energy storage efficiency while maintaining mechanical performance.[56,57] The final samples with 40% MEPCM in resin exceeded 87 J/g of latent heat storage energy.

Furthermore, simply infusing PCM into 3D-printed lattice structures can significantly enhance energy storage efficiency. A representative example is a study in which 50 g of paraffin wax was injected into AlSi10Mg-0403 aluminum lattice structures (thermal conductivity: 96 W/[m·K]) of various sizes, confirming that the 10 mm-spaced structure exhibited the most uniform temperature distribution (below 8 K) and the fastest charging time (17% reduction).[58] Other studies have experimentally demonstrated that in aluminum body-centered cubic (BCC) lattice structures, the use of paraffin leads to shorter complete melting times of the PCM as the surface area of the structure increases.[59] In addition, research has reported the fabrication of structures using photosensitive resin and polyethylene glycol (PEG) mixed in various ratios and printed with a DLP 3D printer.[60] According to this study, higher PEG content (over 50%) results in more pronounced phase change characteristics. The composites exhibit excellent thermal energy storage properties. In this way, the combination of AM and PCM enables the realization of complex energy storage structures without PCM leakage issues. Meanwhile, when combining lattice structures with PCMs, it is important to consider not only conductive heat transfer but also natural convection during PCM melting. Research has shown that among various unit cell structures, the f2ccz structure demonstrates the best thermal performance per unit mass, attributed to its superior heat transfer characteristics in both conduction and natural convection during PCM melting.[61] The study emphasizes that the convective movement of PCM, considering gravity, is a crucial factor that cannot be ignored in the mechanism of thermal energy storage and heat transfer in PCM-3D structure composites.

In summary, AM technology has brought about transformative changes in the design and fabrication of thermal metamaterials. Although challenges remain—such as minimizing interfacial thermal resistance, optimizing the balance between natural convection and conduction, and developing application-specific materials—the integration of AM with thermal metamaterials is expected to provide innovative solutions in various fields, including thermal pathway design, thermal management for electronic devices, improved building energy efficiency, and renewable energy storage. This will make a significant contribution to the advancement of sustainable energy technologies.

4. Convective heat transfer for thermal management using AM

4.1. Various designs of passive and active cooling heat sinks

Since conductive heat transfer alone is often insufficient for effective thermal energy transport, most thermal management systems rely on convection heat transfer, which transfers heat via fluid motion. Two representative cooling devices that utilize convection are heat sinks and heat exchangers. A heat sink typically employs a pin-fin structure to maximize the contact area with the cooling fluid, thereby enhancing convective heat dissipation to working fluids such as air or coolant. Heat sinks are classified into natural convection (or passive thermal management) and forced convection (active thermal management) depending on whether external energy is used to circulate the fluid. Among them, natural convection is a cooling method where fluid motion is driven by the density variations within the fluid itself, made by temperature gradients. Passive thermal management is considered a free-source cooling mechanism as it operates naturally without requiring external power. Moreover, it offers the advantage of being silent due to the absence of externally powered systems. However, the convection heat transfer coefficient in passive systems is relatively low, which limits their broad usability.[62] For the extended applications, forced convection cooling (or active cooling) methods are often employed for applications requiring high cooling performance. It is driven by the external pressure or velocity sources, such as fans, pumps, or suction, which include air-cooling techniques as well as methods using liquid coolant.

Recently, AM has emerged as a promising approach for fabricating diverse heat sink structures. AM technologies provide unprecedented design freedom, enabling the diverse control of parameters such as truss shape, sizes, and lengths. It also allows the minimization of the material used, significantly reducing material waste. Thus, extensive structural and performance enhancements are being actively explored to improve convective heat transfer in AM-produced devices. To enhance cooling efficiency, recent research has focused on: (i) optimizing structural geometries such as cubic, truss, or BCC cells; (ii) refining pin-fin arrays; and (iii) exploring alternative heat sink materials.

In the early stages of heat sink research utilizing AM, most studies focused on structural modification using the L-PBF technique. In particular, many studies aimed to enhance cooling performance by increasing surface area through the manipulation of complex shapes and structures that were previously unmanufacturable before the advent of 3D printing, by adjusting cell structure, size, and geometry (Figure 4). Shamvedi *et al.*[63] fabricated a compact, lightweight, and efficient heat sink by increasing the surface area of lattice structures within a constant heat sink volume, simultaneously optimizing the lengths of the fins. Lorenzon *et al.*[64] developed BCC truss structures with various truss cross-sectional shapes, including circular, elliptical, droplet, and cam shapes, systematically controlling their sizes to achieve enhanced thermal performance (Figure 4A). Tseng *et al.*[65] created five distinct BCC porous truss configurations and experimentally validated their thermal performance under liquid flow cooling conditions.

In addition, significant research has been dedicated to optimizing pin-fin array configurations to enhance heat dissipation performance under natural convection conditions. Lazarov *et al.*[66] utilized L-PBF with aluminum to precisely control the size and arrangement of pin fins, achieving superior passive cooling performance in LED applications. Their optimized pin-fin designs outperformed traditional lattice structures by more than 21%, effectively doubling the life expectancy of the LED devices and reducing operational costs by approximately 50%. In addition to L-PBF, alternative AM techniques have also been explored for fabricating heat sinks. Notably, AM has been actively applied to ceramic-based heat sink designs. Ho *et al.*[67] employed a photopolymerization-based AM method to fabricate complex structures such as honeycomb, Kelvin cells, octet-truss lattices, and mini-gear configurations using ceramic fillers. Similarly, Sheng *et al.*[68] developed a heat sink composed of aluminum nitride powder, achieving structures characterized by robust mechanical properties, high thermal conductivity, and uniform microstructures.

Meanwhile, research has explored modifying the material composition of heat sinks. Traditionally, heat sinks rely on metals due to their inherently high thermal conductivity, which is essential for efficient heat conduction. However, metals typically introduce substantial weight, prompting increased demand for lighter or composite materials.[69] Consequently, polymer composites infused with thermally conductive fillers have garnered attention. Huttunen *et al.*[70] developed heat sinks using thermally conductive plastic filaments, achieving high thermal conductivity coupled with low electrical conductivity, which reduced thermal resistance by approximately 10–20% compared to conventional resin-based heat sinks (Figure 4B). Timbs *et al.*[71] produced heat sinks utilizing polymer filaments loaded with diverse fillers, such as carbon, copper, and bronze. Their study investigated heat sinks designed with straight and oblique fin geometries, comparing their thermal resistance, pressure drop, and heat dissipation

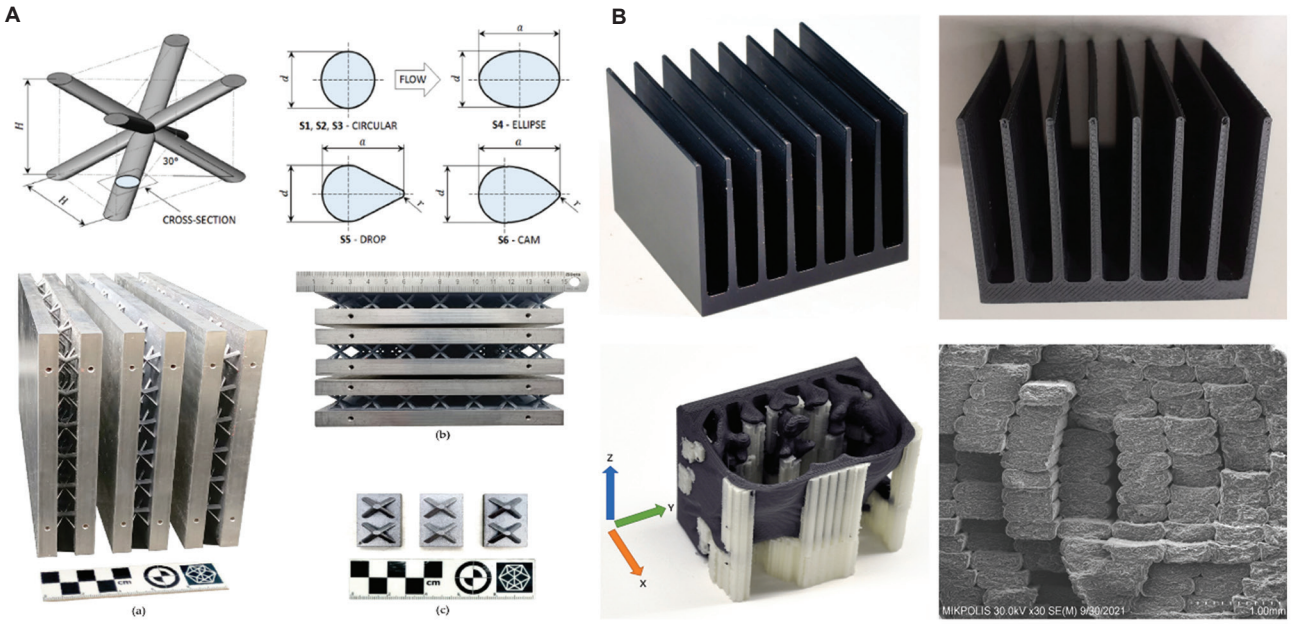

Figure 4. Additively, manufactured heat sinks improve convective heat transfer. (A) Four different cross-sectional fin shapes—circular, elliptical, drop-shape, and cam—were fabricated into real-scale heat sinks with various fin diameters.[64] Copyright © 2024 Luca Casarsa *et al*. Reproduced with permission from author(s). (B) Images of aluminum-based (upper left) and Ice9 Rigid Nylon-based (upper right) heat sinks fabricated via additive manufacturing, and SEM image of the internal layer structure of the Ice9 Rigid Nylon material (lower right).[70]

performance. Collectively, these studies highlight the promising potential of polymer-based heat sinks.

4.2. Micro/mini channel heat sink (MCHS) and TPMS heat sink

In addition to macro-scale thermal management, numerous studies have focused on micro-scale heat dissipation utilizing fluid channels. Particularly in microelectronics, there is significant interest in efficiently removing heat generated within confined spaces. Coolant-based liquid cooling methods are increasingly preferred over traditional air cooling due to their superior heat removal capabilities from the heat source to the surrounding environment. Consequently, extensive research has been conducted on increasing the surface area through micro- and mini-sized channels to enhance liquid cooling efficiency. In addition, the precision capabilities of AM have facilitated the fabrication of intricate micro-scale structures, previously unattainable through conventional manufacturing methods. Thus, current AM-based studies in this area primarily focus on two aspects: (i) the creation of microscale porous structures or channels to enhance convective heat transfer, and (ii) the development of TPMS structures that enable precise control over fluid flow paths, allowing fluids at different temperatures to flow simultaneously without mixing. This part will examine these studies in greater detail, highlighting their contributions and potential applications.

MCHS typically refer to channel structures with hydraulic diameters < 1 mm, enabling significantly higher heat transfer coefficients by minimizing boundary layers compared to larger, conventional heat sink channels. Due to their large surface area-to-volume ratios, these microchannels are extensively employed in compact micro devices, characterized by reduced heat exchanger sizes, minimized material usage during manufacturing, and decreased refrigerant requirements.

Ventola *et al.*[72] were among the first to introduce artificial surface roughness at the microscale, finding that rough-finned surfaces exhibited superior thermal performance (Figure 5A). Subsequently, Kirsch *et al.*[73] investigated microchannel pin-fin arrays with four distinct configurations, concluding that increased surface roughness notably amplified friction factors more than improved heat transfer when compared to smooth pin-fin arrays. Collins *et al.*[74] developed microchannel heat sinks with porous surfaces containing thermally conductive internal fins, which were benchmarked against manifold microchannel designs, achieving a thermal resistance reduction of approximately 17% and a pressure drop reduction of 28%.

Research has also expanded beyond basic pin-fin microchannels by integrating microjets to further enhance convection performance. Kempers *et al.*[75] fabricated hybrid microchannel-microjet heat sinks using a layer-by-

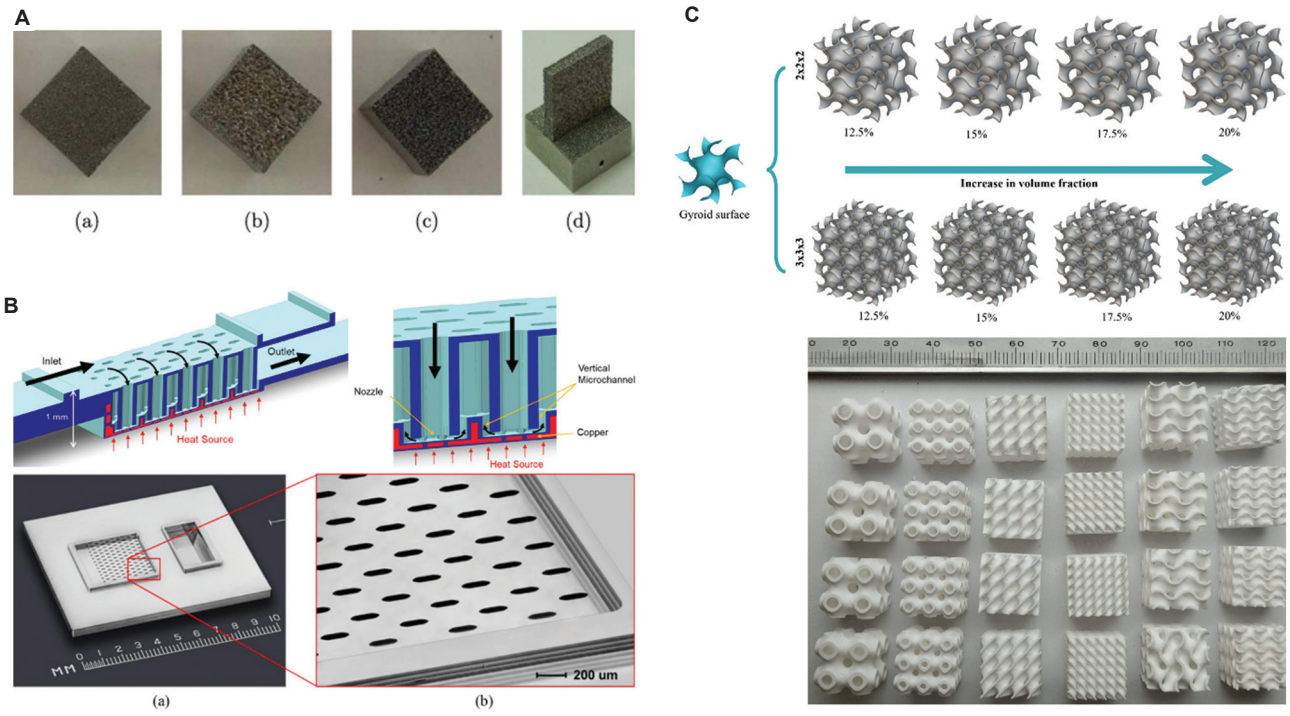

Figure 5. Micro-nanostructures and periodic cell design for enhancing convective heat transfer using additive manufacturing. (A) AlSiMg alloy heat sink manufactured by laser powder bed fusion (L-PBF) method with an artificial surface roughness.[72] (B) Microchannel pin-fin structure incorporating with microjet heat sink.[75] Copyright © 2020 Kempers *et al.* Reproduced with permission from authors(s). (C) Six different triply periodic minimal surface structures by controlling the volume fraction.[77]

layer electrodeposition approach, subsequently comparing performance with previous studies (Figure 5B). In addition, Xu *et al.*[76] explored pulsating flow conditions to enhance secondary flows and vortex formation within a three-layered microchannel heat sink, systematically analyzing the resulting flow characteristics and their impact on thermal performance.

Previous studies primarily focused on single-phase fluid flow within a single-channel configuration for heat transfer. In contrast, TPMS structures enable simultaneous, separate fluid flows at different temperatures within a single integrated design. TPMS structures comprise mathematically defined surfaces characterized by complex topologies, dividing a 3D space into two or more interconnected yet non-intersecting continuous domains. Such configurations have demonstrated substantial improvements in single-phase heat transfer efficiency. Moreover, due to their high surface density, high permeability, and optimal thermal conductivity, TPMS structures are not limited to heat sink applications but extend to fluid mixers, mold cooling modules, and other thermal management applications. Santos *et al.*[77] presented six different geometries and volume fractions of TPMS structures fabricated using aluminum-alumina composites, which show high compressive strengths with an energy absorption behavior (Figure 5C). Yan *et al.*[78] investigated gyroid TPMS structures, showing a significant reduction in pressure drop—up to 40%—through surface polishing. Similarly, Raafat *et al.*[79] developed a TPMS-based porous pin-fin heat sink structure, which exhibited enhanced Nusselt numbers with reduced channel blockage facilitated by the porous configuration. They verified that secondary cooling flows induced within the porous region effectively prevented disruption of the thermal boundary layer. Although TPMS structures are typically fabricated using metallic materials, such as AlSi10Mg alloys, recent studies have demonstrated their potential when produced using polymeric materials. For instance, Oh *et al.*[15] successfully fabricated polymer-based TPMS structures using the DLP printing method, conducting pressure-drop evaluations and detailed flow visualization studies to analyze their fluid flow characteristics. Especially, the transparent characteristic of polymer heat exchangers allows for easy visualization of temperature distribution at the inlet and outlet, either by direct observation or through IR imaging. This feature also offers the advantage of addressing the high-cost issues associated with conventional metal-based AM.

4.3. Structural optimization in AM

There is a growing demand for structures to be lightweight and material-efficient, minimizing material usage while

maintaining performance. However, optimizing the geometry of heat sinks to achieve the best thermal performance remains a critical challenge. Previous studies have predominantly relied on experimental approaches to fabricate and evaluate heat sinks and heat exchangers, systematically comparing performance to identify optimal structural configurations. Parameters such as cell type, porosity, and functional gradients are highly tunable through implicitly defined surfaces, including TPMS and MCHS geometries. Accordingly, numerical approaches and machine learning techniques are increasingly being used to optimize heat sink designs. Employing numerical simulations before actual manufacturing presents significant advantages, as it allows for parameter optimization of processing methods, printing techniques, and structural characteristics—such as thickness, size, and material selection—thus significantly reducing costs and minimizing material waste. Therefore, this part aims to comprehensively explore three prominent optimization methodologies used in AM-based heat sink and exchanger design: (i) geometry-based optimization, (ii) topology optimization, and (iii) machine learning-based optimization (Table 2).

Geometry-based optimization actively involves adjusting parameters such as pin-fin size, shape, and spacing to achieve optimal thermal performance and pressure drop characteristics. Ning *et al.*[80] numerically investigated fin structures, specifically twisted and rectangular fins, to evaluate their thermal performance and associated pressure drop, highlighting the potential of structural optimization through simulations by predicting inlet and outlet fluid-flow temperatures. Similarly, Ozguc *et al.*[81] employed computational fluid dynamics (CFD) simulations for optimizing pin-fin geometries, including size and shape, within water and ethylene glycol coolant mixtures, applying a gradient-based multi-objective optimization method. Kong *et al.*[82] conducted CFD-based thermal-fluid simulations on heat sinks combining pin fins and plate structures to determine configurations with optimal thermal resistance, pressure drop, and coefficient of performance, and successfully predicted overall thermal resistance and pressure drop. Bacellar *et al.*[83] proposed an optimum design by varying the channel and fin geometries of the microchannel heat exchangers into four types—round, elliptical, eye-shaped, and airfoil (leading and trailing shape). This approach resulted in more than a 50% reduction in size, material usage, and pressure drop.

Likewise, geometry-based optimization has also been extensively applied to TPMS structures using CFD methodologies. Raafat *et al.*[79] incorporated pin-fin arrays into TPMS-based structures, developing configurations capable of reducing pressure drop compared to conventional designs. Their optimized structures demonstrated high surface-to-area ratios, targeted enhanced Nusselt numbers, and maintained balanced hydrothermal performance through porous-like topologies that minimized channel blockage. Tang *et al.*[11] introduced a novel lattice-control method explicitly tailored for optimizing gyroid-type TPMS, accompanied by corresponding mathematical equations, and systematically compared simulated and experimental results to evaluate convective heat transfer performance and flow resistance. Further research efforts have focused on systematically analyzing the heat dissipation performance of various TPMS geometries to identify optimal configurations. Liu *et al.*[84] compared heat transfer and flow characteristics of four distinct TPMS structures (i.e., gyroid, primitive, diamond, and I-graph-wrapped package) through numerical simulations. Based on comparative performance results, the most effective TPMS structure was selected and validated experimentally under natural and forced-air convection conditions.

Meanwhile, topology optimization is a numerical approach employed to systematically optimize material distribution and structural configuration within a defined design domain. It aims to minimize material usage and strain energy while preserving mechanical integrity and enhancing overall performance. This method involves defining specific design variables, an objective or cost function, and appropriate constraints to achieve targeted design outcomes effectively. Tan *et al.*[85] applied topology optimization to compare four distinct microchannel heat sink designs—veiny, lateral veiny, snowflake-shaped, and spider-netted structures—numerically determining the optimal geometric parameters. Ozguc *et al.*[86] conducted topology optimization of microchannel heat sinks using a homogenization approach, specifically employing Pareto optimization to identify optimal configurations, including grid cell sizes, fin thickness, and pin-fin array layouts. Orakwe *et al.*[87] evaluated four different cold-plate designs: A conventional serpentine configuration, a geometrically similar replica of a reference design, and two hybrids, topologically optimized (TopOpt) lattice-based heat sinks. Their research utilized functionality-driven designs with AM frameworks, incorporating numerical methods based on field-driven implicit equations to optimize side-wall geometries within computer-aided design models. In addition, recent topology optimization approaches incorporate bio-inspired structures. For instance, Han *et al.*[88] developed a heat sink inspired by spider-web topology, targeting reduced temperature differences and pressure drops. To enhance heat-transfer performance and mitigate hot-spot temperatures, this study utilized staggered inlet and outlet configurations, ultimately selecting a three-inlet and three-outlet arrangement for

Table 2. Summary of AM-based structural optimization

Optimization methodology	Printing method	Material	Shape	Method	Working environment	Performance evaluation	Optimization target	References
Geometry optimization	L-PBF	Stainless steel	Twisted fin, rectangular fin	Numerical CFD, MOGA	DI water, oil, air	Thermal, pressure drop, COP	Optimal performance with fabrication capability	80
	L-PBF	AlSi10Mg	Rectangular pin fin	Numerical CFD	Water/ ethylene glycol mixture	Thermal, pressure drop	Minimizing thermal resistance with optimized pressure drop	81
	L-PBF	AlSi10Mg	Pin fin, plate	Numerical CFD	DI water	Thermal, pressure drop, COP	Optimal cooling performance in a high-temperature fluid environment	82
	L-PBF	AlSi10Mg	Gyroid TPMS	Numerical	Air	Thermal, flow resistance	Optimal thermal performance and pressure drop through lattice deformation	11
	L-PBF	AlSi7Mg	Gyroid, primitive, diamond, I-graph-wrapped package TPMS	Numerical CFD	Air static, flow	Thermal	Optimal thermal performance in various conditions	83
Topology optimization	-	6063 aluminum base	Ternate veiny, lateral veiny, snowflake shape, spider netted microchannel	Numerical	Water	Thermal	Optimal cooling performance in a high-temperature fluid environment	84
	L-PBF	AlSi10Mg	Square pin fin	Numerical CFD	Water	Thermal, pressure drop compared with the simulation result	Thermal performance enhancement and pressure drop optimization	85
	L-PBF	Copper	TPMS	Numerical CFD	Water	Thermal, pressure drop	Optimal thermal performance with fabrication capability	86
AI-driven optimization	L-PBF	AlSi10Mg	Straight, wavy fin	Deep reinforcement learning, MOGA, CFD	Air	Thermal, flow resistance, process availability	Optimal performance with fabrication capability	87
	L-PBF	AlSi10Mg	Rectangular, straight mini channel	Neural network, genetic algorithm	Water	Pressure drop	Optimal thermal performance in various conditions	88
	L-PBF	AlSi10Mg	Mini channel	Neural network, CFD	Water	Pressure drop	Optimal thermal performance in various conditions	89
	L-PBF	AlSi10Mg	Grid, rhombic	ANN, k-NN, SVR, ensemble ANN, ensemble k-NN, ensemble SVR	Air	Thermal performance prediction	Optimal thermal performance prediction of a complex structure	90

Abbreviations: AI: Artificial intelligence; AM: Additive manufacturing; ANN: Artificial neural network; CFD: Computational fluid dynamics; COP: Coefficient of performance; DI: Deionized; k-NN: k-nearest neighbors; L-PBF: Laser powder bed fusion; MOGA: Multi-objective genetic algorithm; SVR: Support vector regression; TPMS: Triply periodic minimal surface.

optimal performance. Helmholtz filtering combined with hyperbolic sine projection methods was integrated into the topology optimization process to further refine and achieve the desired outcomes.

However, predicting performance through numerical approaches to find an optimal point often does not precisely match real-world results. For instance, simulation environments typically apply highly constrained boundary conditions, which rarely occur in practical scenarios. Furthermore, purely simulation-based methods are limited in their capacity to generate novel, data-driven structures. To overcome these limitations, machine learning methods have been increasingly adopted. Artificial intelligence (AI)-driven optimization methods significantly enhance the efficiency and reliability of heat sinks, providing scalable solutions particularly suitable for high-power electronics. Specifically, the adoption of AI in AM supports various aspects, including design optimization, quality assurance, process optimization, and material development. Robertson *et al.*[89] employed an AI-driven optimization framework, combining deep reinforcement learning with a multi-objective genetic algorithm (MOGA), to determine optimal geometric parameters of heat sink fins, such as fin spacing, height, thickness, and base thickness, thus supporting both design and quality assurance goals. Wang *et al.*[90] utilized machine learning to facilitate design optimization, leveraging genetic algorithms to accumulate structural optimization data. They subsequently predicted performance evaluation criteria and heat-transfer efficiency using neural network-based predictions. In addition, Wang *et al.*[91] applied machine learning methods to estimate pressure-drop performance of heat sinks, validating their predictions against numerical simulations and experimental results for optimized performance. Commonly employed machine learning approaches involve neural networks and regression-based models, though various other predictive models have also been explored. Aksoy *et al.*[92] comparatively evaluated six different machine learning algorithms: Artificial neural network (ANN), k-nearest neighbors (k-NN), support vector regression (SVR), ensemble ANN, ensemble k-NN, and ensemble SVR. These methods utilized inputs such as time, current, gate voltage, and temperature to estimate heat sink temperatures, comparing predicted results with experimental data.

Moreover, machine learning methods have been extensively utilized in process optimization. Thakur *et al.*[93] studied optimal laser power, scanning speed, and hatching spacing parameters for 3D printing of heat sinks, subsequently validating residual stress and distortion predictions through simulations and real tests. They further developed data-driven mathematical relationships between residual stress and porosity using machine learning techniques, particularly multiple regression analysis and gray relational analysis. Through this model, the relationship between printing parameters and residual stress was systematically identified, facilitating comprehensive structural and manufacturing process optimization for heat sinks.

AM has enabled significant enhancement in the thermal performance of convection-based cooling systems. In particular, the fabrication of complex structures such as pin-fin arrays, MCHS, and TPMS geometries has become readily achievable. We summarize recent studies on active and passive cooling strategies employing AM heat sinks and heat exchangers. Furthermore, detailed attention is given to MCHS and TPMS structures that enhance convection performance through increased surface area. Moreover, the design and performance of these cooling systems can be further optimized using numerical simulations and machine learning techniques, which help to minimize time-consuming trial-and-error processes and material waste.

4.4. Boiling heat transfer for thermal management using AM

In previous examples involving MCHS and TPMS structures, cooling was achieved using oil, gas, or water, using only single-phase flow within the system. Such systems rely on natural or forced convection mechanisms, which exhibit heat transfer coefficients in the range of approximately 0.001–10 W/(cm^2·K).[94] However, high-performance systems such as radar modules, turbine blades, advanced electronics, and aerospace applications demand the removal of heat fluxes in the range of 25–1000 W/cm^2 or even higher, while maintaining material temperatures within prescribed safety limits. Under these extreme conditions, single-phase convection becomes insufficient for effective thermal management. As a result, two-phase boiling heat transfer has gained significant attention in recent research as a promising approach for dissipating high heat fluxes more efficiently. This method leverages the latent heat of vaporization and the dynamic interaction between liquid and vapor phases to achieve enhanced heat transfer performance. In phenomena such as pool boiling, staged mechanisms such as nucleation, bubble detachment, and rewetting further enhance heat transfer.

Single-phase and two-phase (liquid-vapor) heat transfer exhibit fundamental differences in their underlying mechanisms, and these differences are particularly apparent during boiling. In systems where the fluid exists in only one phase, either liquid or gas, heat is transferred primarily by conduction and convection. Heat is first conducted from the wall surface to the fluid, and it is then

transported within the fluid by natural or forced convection driven by temperature gradients. Energy transfer in this case relies mainly on sensible heat, the energy associated with a change in fluid temperature. By contrast, two-phase boiling heat transfer occurs when liquid and vapor coexist, and heat transfer is dominated by the formation and motion of bubbles generated as liquid evaporates from an overheated surface. This process involves latent heat associated with the phase change, making it far more efficient at transferring heat. In phenomena such as pool boiling, staged mechanisms such as nucleation, bubble detachment, and rewetting further enhance heat transfer.

4.5. Pool boiling

Pool boiling is a boiling phenomenon that occurs when a stationary liquid is heated and begins to evaporate. It is widely used in various thermal management systems that require high heat flow rates because it enables high heat transfer performance and stable operating temperature maintenance. Depending on the temperature of the wall, the process of pool boiling is categorized into four regimes: free convection, nucleate boiling, transition boiling, and film boiling (Figure 1A). In the free-convection stage, the surface temperature is only slightly above the liquid's saturation temperature, so the liquid is warming, but no bubbles have formed. In the process of nucleate boiling, the surface temperature increases to a sufficient degree to cause the formation of bubbles on the surface. This results in the occurrence of latent heat transfer, which is characterized by its high efficiency. Consequently, the maximum HTC is attained. Subsequently, transition boiling occurs when bubble coalescence and a vapor film form due to excessive bubble generation. In this phase, heat transfer is unstable and can decrease rapidly. Eventually, when the surface is covered with a continuous vapor film, known as film boiling, heat transfer efficiency is greatly reduced. This boiling process is divided into three points. The first point is known as the onset of nucleate boiling (ONB), which denotes the first point of bubble formation. The second is the point at which the maximum heat flux is reached in the nucleate boiling region. After this point, heat transfer decreases sharply due to coalescence and the vapor film. The third is the Leidenfrost point. Vapor film completely covers the wall surface, preventing contact with liquids and necessitating heat to transfer by means of radiation and vapor conduction. To improve pool boiling performance, it is important to precisely control bubble dynamics. By controlling bubble nucleation sites, detachment, and coalescence, both HTC and CHF can be improved simultaneously. Surface microstructure design can increase nucleation site density and wettability, thereby delaying CHF.

4.5.1. Bubble guide using AM

By enabling free design and single-process fabrication of micro-millimeter-scale structures, AM is changing the paradigm of pool boiling design.[95] L-PBF can be used to easily implement complex structures such as a vapor-guiding structure, a hollow conical structure, and a re-entrant microchannel structure. Structures similar to those mentioned increase bubble nucleation density, organize vapor-liquid separation pathways, and promote capillary pressure-based liquid replenishment, significantly enhancing HTC and CHF.[96] Taking advantage of L-PBF design flexibility, Shim *et al.*[97] showed the design and fabrication of a vapor-guiding structure. This structure effectively suppressed lateral coalescence by inducing vertical growth and stable detachment of bubbles and smoothly maintained liquid replenishment to prevent the formation of localized dry areas. Compared with a plain surface, this structure achieved a 90% increase in HTC and a 60% improvement in CHF. Another study attempted to control bubble growth using a bubble guide, as shown in Figures 6A and B.[98,99] Pi *et al.*[100] fabricated a re-entrant microchannel structure using L-PBF. This design incorporates an internal mechanism that captures the bubbles within the structure and directs them towards a narrow outlet at the upper point. This structure improved the heat transfer coefficient by at least 10% and up to 330% compared to flat surfaces. In addition, ONB temperature was significantly lowered, greatly improving the initial boiling transition conditions. Hayes *et al.*[101] fabricated a hollow conical structure for regulating flow via metal AM. The hollow conical body is equipped with vapor-exhaust outlets on the top and side walls. This structure allows the self-organization of vapor and liquid flow paths in accordance with the dimensions and relative positioning of these outlets. When this structure was applied, the heat transfer coefficient improved by up to 400% compared to a metal plane, and the CHF improved up to 200%. These L-PBF-based structures achieved higher performance than existing flat structures by effectively controlling the bubble dynamics, such as the location of bubble generation, growth direction, departure timing, fusion prevention, and liquid replenishment path.

4.5.2. Surface roughness modification

Another advantage of the L-PBF process is the high roughness of the surface formed during the fabrication process. A semi-molten metal powder forms on the surface of metals manufactured using L-PBF.[102] This creates a roughness ranging from micrometers to tens of micrometers.[96] This surface roughness increases the density of bubble nucleation sites, promoting initial bubble formation and contributing to improved heat

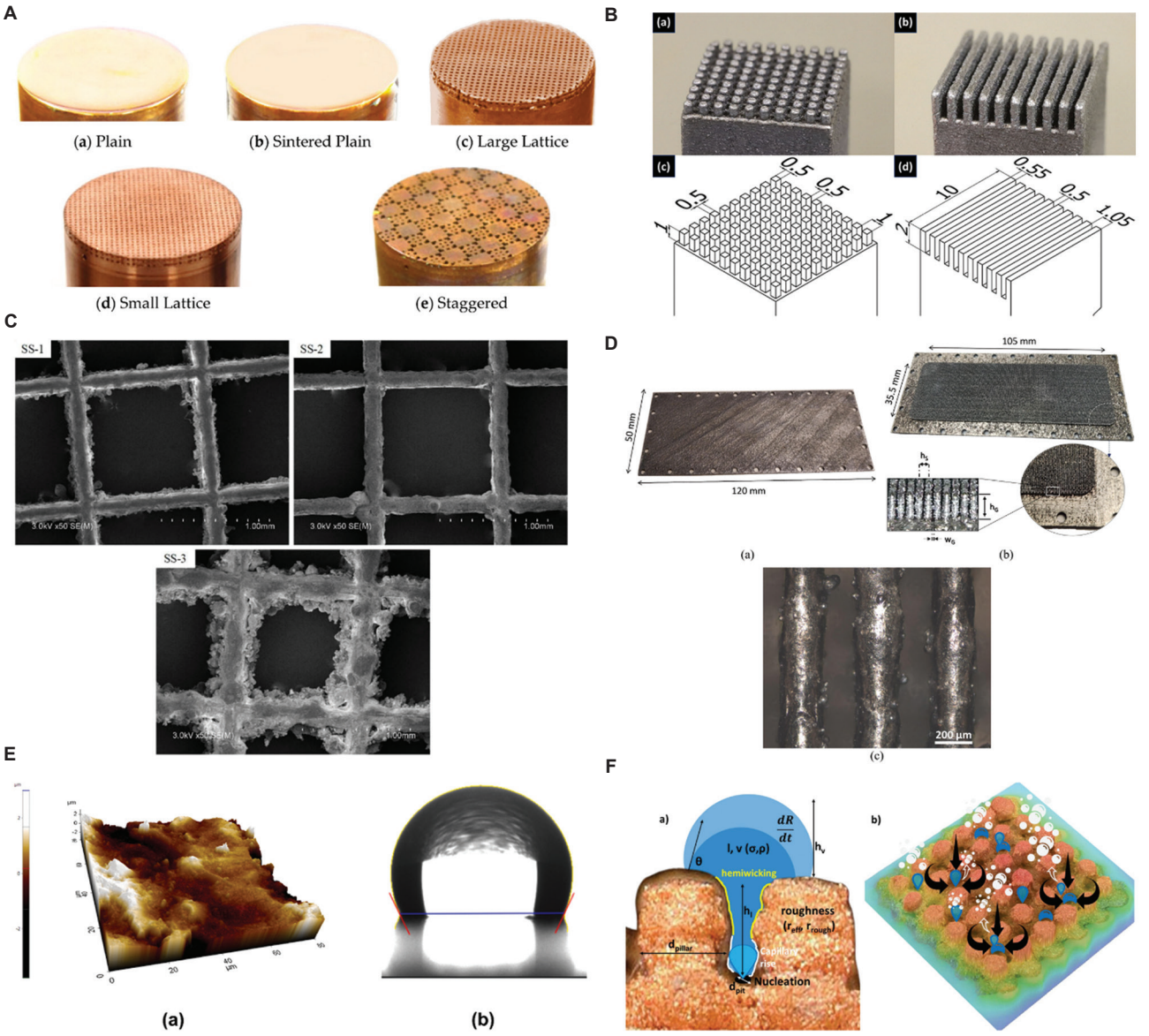

Figure 6. Pool boiling enhancement using additive manufacturing. (A) Vapor- guiding structure for bubble path.[98] (B) Images of different fin structures using L-PBF.[99] Copyright © 2025 American Chemical Society. Reproduced with permission of the American Chemical Society. (C) SEM image of a porous structure with different layer thickness fabricated by L-PBF.[105] (D) Bottom plate of heat sink using L-PBF.[104] Copyright © 2025 Kempers *et al*. Reproduced with permission from the author(s). (E) Surface roughness and contact angle of L-PBF surface.[103] Copyright © 2023 Kim *et al*. Reproduced with permission from the author(s). (F) Roughness and bubble guide using fused deposition modeling.[107] Copyright © 2025 Gupta *et al*. Reproduced with permission from the author(s).

transfer coefficients.[103] There are studies that have achieved improved HTC and CHF performance using only L-PBF-based roughness without a separate structural design.

Research has also shown that the L-PBF-based roughness across an entire macro-fin surface can enhance performance. As shown in Figure 6C and D, surface roughness can be increased using AM.[104,105] Lum *et al.*[106] showed various macro-fin geometries produced by L-PBF. The surface of the fin forms a micro-cavity with an average Ra of 10 µm due to the layer-by-layer method and partially sintered powder. The improved wettability promotes the formation of active nuclei on the sidewalls and top of the pins, causing bubbles to form on the whole structure. As a result, the emerging bubble coalesced with the growing bubble at an early stage, shortening the detachment cycle and increasing the heat transfer coefficient by up to 67%.

L-PBF-based roughness improves performance, but additional processing can further enhance pool boiling

performance. As illustrated in Figure 6E and F, surface roughness and contact angle can also be reduced using SLM.[103,107] Lum *et al.*[108] achieve a rough, porous layer with an average Ra ≈ 21 μm that boosts capillary pressure and secures liquid-spreading pathways using L-PBF. Chemical etching and boehmite oxidation lower the static contact angle from 44.7° to nearly 0°. This causes rapid re-wetting and increases the active nucleation density, allowing bubbles to form and escape quickly. Even without post-processing, the rough L-PBF surface improved HTC by 32.5% relative to Al 6061. Moreover, the maximum HTC increased by 103.8% with surface treatment.

Meanwhile, layer-by-layer processes such as FDM also enhance wettability. Elkholy *et al.*[109] proposed that PLA structures layered using the FDM naturally form a porosity of 11% because of inter-layer gaps. This gap creates a fine capillary network that improves surface wetting. This internal wicking ability reduced the contact angle to 34.5°, allowing the surface to wet easily and lowering the temperature required for the ONB. A significant improvement of up to 81% was achieved in terms of the HTC, attributed primarily to the integrated mechanism of capillary-driven liquid replenishment and low contact angle.

4.6. Flow boiling

Flow boiling is a complex heat transfer phenomenon in which a fluid flows along a heated surface and its phase changes from liquid to vapor. The mechanisms of heat transfer act in accordance with the flow behavior and phase change of the fluid. A key difference from pool boiling is that heat transfer by forced convection also occurs. Therefore, flow boiling regimes are classified by the liquid-vapor distribution (Figure 1A). When vapor quality is low, a continuous liquid phase containing small, scattered bubbles forms bubbly flow. As the temperature of the wall increases, the bubbles expand and merge, causing the slug flow to alternate between vapor slugs and liquid slugs. This provides strong turbulence and enhances heat transfer. As the steam quality increases, an annular flow is formed in which the steam dominates the center, and a thin liquid film forms on the wall. This maintains a high heat transfer coefficient, but when the heat flux increases rapidly and the liquid film disappears, it changes to a droplet flow in which the liquid droplets move with the steam. Finally, the wall dries out, and heat transfer decreases rapidly. In order to achieve efficient heat transfer in this flow boiling process, it is very important to precisely control bubble dynamics, such as bubble formation, growth, and separation, as well as forced convection flow. To improve these factors, structural designs that uniformize the flow distribution within the channel and surface modifications that improve wettability are being actively researched.

4.6.1. Flow control

As mentioned earlier, L-PBF offers a high degree of manufacturing flexibility, enabling complex and precise internal flow structures. These advantages are particularly beneficial in flow boiling. The coexistence of vapor and liquid due to fluid boiling creates a multiphase flow environment, which increases fluid heterogeneity and can cause problems such as localized dry-out and overheating.[110] To solve these problems, it is essential to design a flow path that ensures spatial uniformity of the inflowing fluid and effectively controls the vapor-liquid mixture state. L-PBF-based structural design is a suitable method for meeting these requirements, as it enables high-resolution implementation of lattice, TPMS, and gradient-based flow control structures, thereby enabling simultaneous improvement of flow uniformity and heat transfer coefficients (Figure 7A and B).[10,57]

Figures 7C-E show that various structures can be produced using L-PBF.[103,111,112] Wong *et al.*[113] fabricated a 3D porous metal structure. The gradient structure is designed to gradually reduce the cross-sectional area of the flow, thereby increasing the flow velocity as the flow progresses and implementing a mechanism that enhances fluid mixing. Inside the structure, nucleate boiling was dominant due to bubbly flow and churn flow. Among the different TPMS structure types surfaces, the gyroid is too complex to fabricate by conventional methods. However, as shown in Figure 7B, it was possible to fabricate a gyroid-based heat exchanger using L-PBF.[10] Because of the gyroid's continuous, periodic curved surfaces, the fluid is uniformly distributed throughout the exchanger. As flow rate increases, the heat transfer coefficient rises to 450 W/(m^2·K), and the device achieves more than a 50% mass reduction relative to a conventional shell-and-tube heat exchanger while actually improving thermal performance. Flow-boiling conditions involve rapid property changes accompanying vapor-liquid phase change, increasing design complexity. As shown in Figure 7F, structural optimization studies have therefore been undertaken.[114] Zhou *et al.*[115] obtained a root-like branching pin fin shape through 3D VOF (Volume of Fluid)-based numerical modeling. Simulations showed that, compared to a baseline configuration, the optimized structure delayed ONB through higher convective surface area and more uniform flow distribution, yielding up to an 87% increase in average HTC. A subsequent study fabricated the optimized design with DMLS.[116] The optimized heat sink reduced the ONB by up to 6.6 K compared to the baseline configuration, enabling rapid nucleate boiling. In addition, the flow visualization results showed that bubbly flow was highly stable and

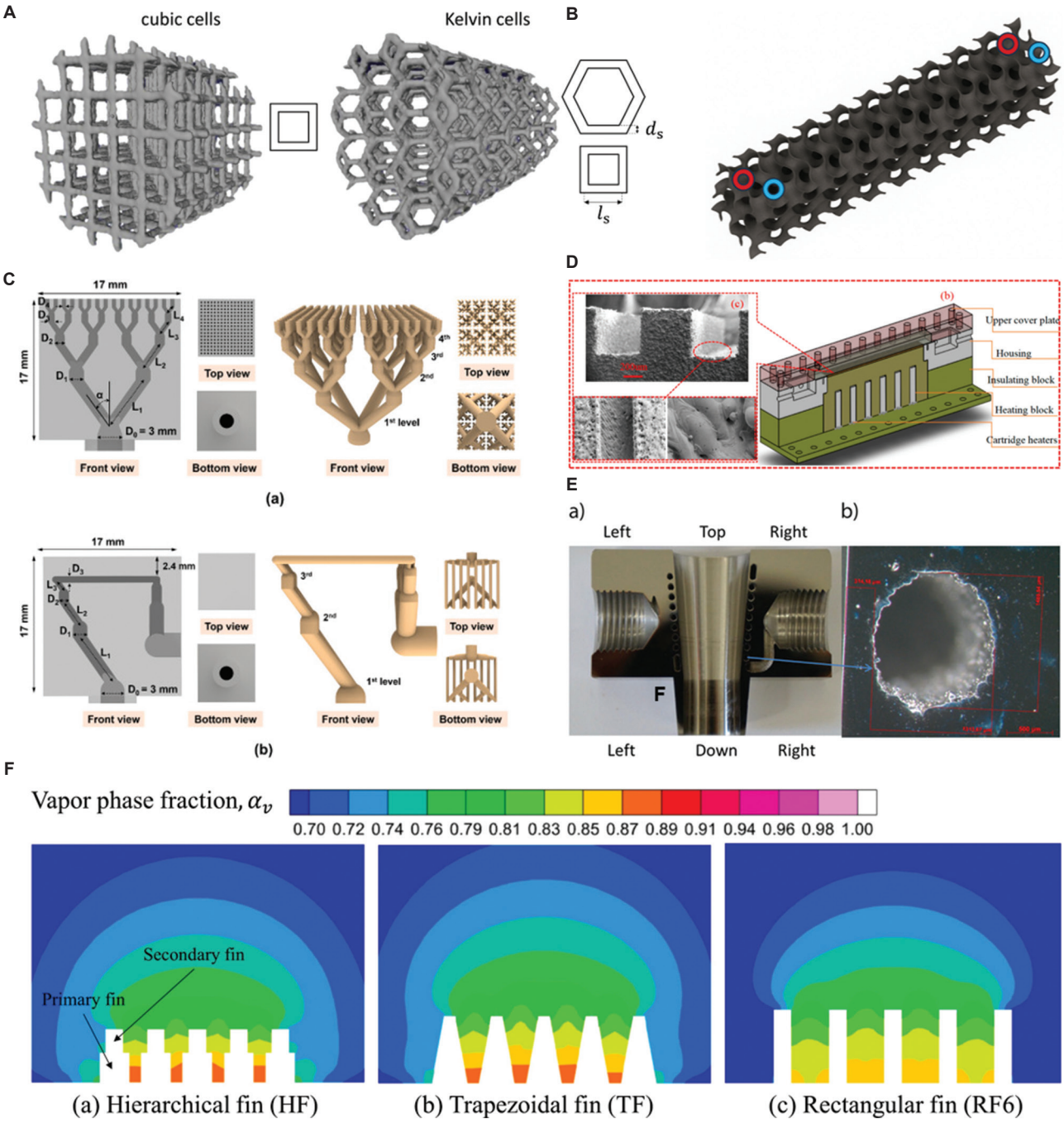

Figure 7. Flow boiling enhancement using additive manufacturing. (A) Flow boiling enhancement using additive manufacturing. (A) Computed tomography scan image of cubic cell and Kelvin cell fabricated using laser powder bed fusion (L-PBF).[57] (B) Illustration of Gyroid structure (L = 199.5 mm, H = 40.5 mm, and W = 41.51 mm).[10] (C) Design schematic image of a microchannel heat exchanger using L-PBF.[103] Copyright © 2023 Kim *et al*. Reproduced with permission from the author(s). (D) Schematic diagram of a mini-channel heat sink.[111] (E) Images of 3D-printed mini channel evaporator.[112] (F) Vapor phase fraction simulation for fin structure.[114] Copyright © 2025 Park *et al*. Reproduced with permission from author(s).

recorded the highest HTC in the slug flow section. L-PBF-based internal flow design effectively suppresses local overheating, dry out, and the resulting deterioration in thermal performance by equalizing fluid distribution in a flow boiling environment. L-PBF will be an effective manufacturing method for developing lightweight, high-efficiency heat exchangers by precisely implementing complex flow channels.

4.6.2. L-PBF roughness modification

Flow boiling is influenced by bubble dynamics such as bubble nucleation, growth, coalescence, and detachment from the channel wall. The microstructure of the surface has a decisive influence on bubble dynamics during this process.[117] Therefore, the unique roughness generated in the L-PBF can be utilized as a functional element directly related to the boiling heat transfer mechanism.[118] Ye *et al.*[119] conducted a study leveraging L-PBF advantages, in which the surface of mini channels forms a structure with particles of 3 μm in diameter and irregular grooves of 20 μm in size due to incomplete melting of the powder. As a result, the average Ra increases by about 40 times compared to Al. This size range coincides with the optimum bubble-nucleus radius for R134a (1–20 μm), increasing the density of nucleation sites and enhancing wettability. In addition, ONB was accelerated by lowering the initial superheat, and the heat transfer coefficient of the channel was approximately 60% higher than that of Al6061. Without separate post-processing, L-PBF roughness can simultaneously increase surface wettability and bubble nucleation density, achieving up to a 50% improvement in thermal performance. However, since the improvement is limited due to the uneven distribution of nucleation sites, additional design optimization is required to precisely control the roughness shape.

4.7. Two-phase thermal management devices

Two-phase thermal management devices can be classified into vapor chambers, flat heat pipes, loop heat pipes, and pulsating heat pipes according to the circulation mechanism of the internal fluid. The most common types are the flat heat pipe and vapor chamber. Both cases use capillary force through a wick structure installed inside to circulate the condensed liquid back to the evaporation section. A loop heat pipe, with a more complex layout, directs vapor and liquid through physically separated channels and uses wick-based capillary action to transport heat efficiently over long vertical distances. In a pulsating heat pipe, the working fluid oscillates in a plug-slug pattern, repeatedly evaporating and condensing to move heat.

4.7.1. Wick structure

Recent advances in AM have enabled the precise design and fabrication of wick structures inside heat pipes and vapor chambers.[120] As shown in Figure 8A, L-PBF makes it possible to form complex capillary pathways, tailor porosity, and produce integrated parts that can be bent.[121] Mezghani *et al.*[122] fabricated a micro-pillar wick that was implemented inside the vapor chamber using the L-PBF process. The wick structure is a cylindrical column with a diameter of several tens of micrometers. This ensures a high specific surface area and uniform capillary paths. Improvement of working-fluid replenishment and nucleation site enhances evaporation performance. This resulted in a reduction in thermal resistance of up to 58.9% compared to commercial vapor chambers. As shown in Figure 8B and C, AM also enables a high-porous wick structure to be fabricated using L-PBF.[123,124] Meng *et al.*[125] proposed a vapor chamber with a composite porous-wick architecture. This structure separates the evaporation, condensation, and liquid return functions, adopting TPMS structures with varying pore sizes for each. Specifically, a hybrid-pore wick was implemented through the differentiation of cell sizes, thereby resolving the trade-off between capillary pressure and permeability. This arrangement lowered thermal resistance by up to 49.6% relative to a conventional single-pore wick. As shown in Figure 8D, another advantage of this arrangement is the integrated design, unlike that achieved with conventional manufacturing methods.[126] Park *et al.*[127] fabricated a cylindrical heat pipe manufactured using the L-PBF method, which also incorporates an integral wick in the bent structure. A hybrid capillary system was realized by incorporating a screen-covered groove structure in the evaporator and a groove wick in the condenser and adiabatic sections. The screen mesh supplies not only a small pore radius to achieve high capillary pressure, but the groove wick provides high permeability for liquid circulation. This configuration reduced thermal resistance by up to 24.2% compared with a homogeneous groove-wick heat pipe and reached a maximum effective thermal conductivity of 25.7 W/(m·K). Thus, AM enables complex wick structures to be realized in a one-step process, achieving superior thermal performance and structural stability compared with assembled or conventional wicks. In particular, the freedom to design and fabricate wick geometry through L-PBF offers great flexibility for capillary-driven two-phase heat-transfer systems.

4.7.2. Wettability modification

L-PBF has been shown to yield surface roughness and wettability, which can contribute to maximizing the functionality of wick structures. The micro-nanoscale textures that inherently form during L-PBF enhance capillary forces and improve contact with the working liquid, enhancing heat-transfer performance.[128] One trade-off is that partially-sintered powder can remain trapped in internal features, making as-built L-PBF parts up to ~7% heavier than their nominal design mass.[129] Despite the slight loss of mass, numerous studies have shown that the improved wettability and capillary pumping effect provided by these micro-nano textures result in excellent heat transfer under conditions of high heat flux or gravitational influence. Such precise control is difficult to

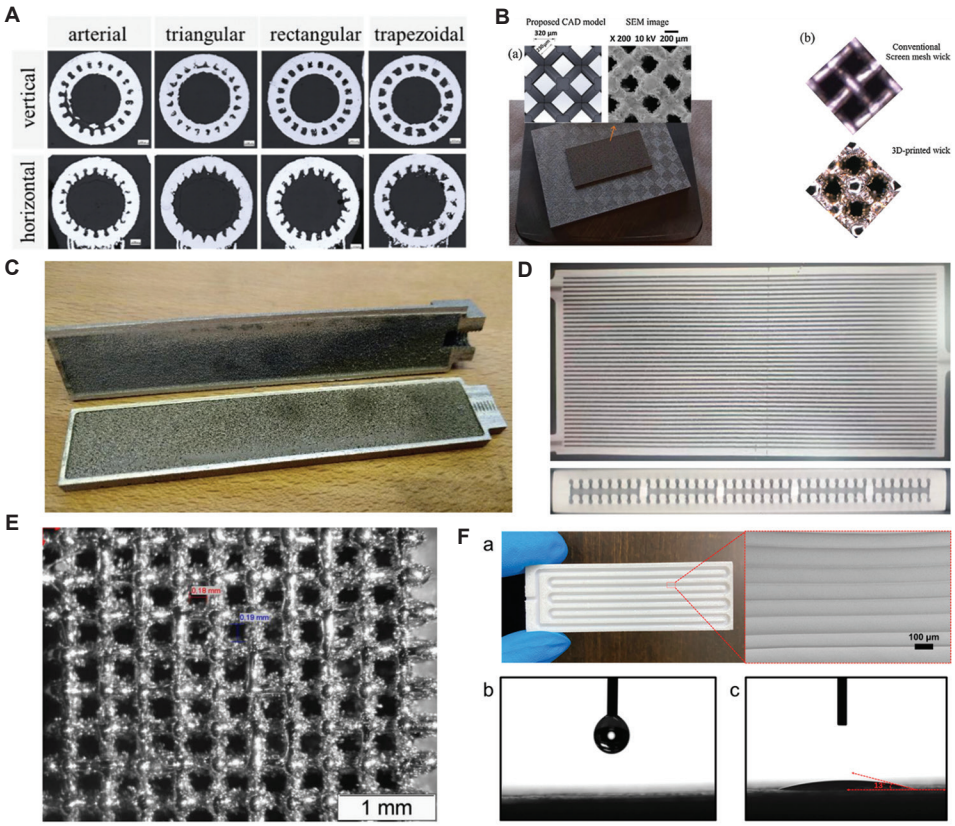

Figure 8. Two-phase heat spreader enhancement using additive manufacturing. (A) Different wick structure using L-PBF.[121] (B) SEM image of porous wick and comparison between conventional and 3D-printed wick.[124] Copyright © 2025 Geurts *et al.* Reproduced with permission from the author(s). (C) Porous wick heat pipe fabricated using L-PBF.[123] Copyright © 2021 R. Kempers *et al.* Reproduced with permission from author(s) (D) Heat pipe with wick structure using L-PBF.[126] (E) Scaffold internal structure for capillary.[130] (F) Photograph and contact angle of Pulsating heat pipe made with AM-based polymer.[133]

achieve with traditional machining or forming processes, which is particularly advantageous in high heat flux conditions or gravity-affected environments. As shown in Figure 8E, wettability is improved due to increased roughness caused by unmelted powders.[130] Yun *et al.*[131] fabricated a flat heat pipe with a groove-pattern wick by exploiting the inherent roughness of L-PBF. It exhibited a thermal resistance of 0.69°C/W and an effective thermal conductivity about 589% higher than that of the same volume of aluminum. These gains are attributed to the increased surface roughness created by L-PBF, which promotes liquid replenishment and increases boiling sites. Roughness can also be tuned by adjusting laser power. Cui *et al.*[132] suggested a porous wick composed of cylindrical-cubic unit cells in a loop heat pipe. Reducing the laser power from 170 W to 125 W left more partially melted particles on the surface, increasing micro-cavities. This increases the porosity to 52% and the capillary absorption to 3.53 g in 2 minutes. With this porous wick, thermal resistance fell by 26.5% compared with a conventional copper-powder wick, and the evaporator temperature dropped about 8.2% lower than that of the copper wick. Both studies confirm that the surface roughness and wettability of L-PBF-fabricated wick structures play a decisive role in enhancing the thermal performance of heat pipes and loop heat pipes. Despite an inherent L-PBF weight gain from trapped powder, the enhanced capillary pumping and liquid spreading still deliver superior heat transfer. These findings highlight that integrated optimization of geometry design, pore-size control, surface-roughness adjustment, and post-processing is crucial for further performance gains.

4.7.3. Polymer-based two-phase thermal management device

Application of AM with polymer materials, unlike L-PBF with metals, offers greater processability and design freedom, along with transparency and weight reduction. It is attracting attention for its potential applications in the precise observation of heat transfer mechanisms and passive thermal management devices for cooling electronic devices. Similar to Figure 8F,[133] Arai *et al.*[134] fabricated a pulsating heat pipe made of transparent

polycarbonate using an SLA-based AM process. With a channel diameter of 0.8 mm and a filling ratio of 30 vol%, it achieved a maximum effective thermal conductivity of 7.0×10^3 W/(m·K). In the small channel, a stable slug flow was seen, and this flow helped with heat transfer efficiency by activating the simultaneous transfer of latent heat and sensible heat between the evaporation and condensation sections. Pulsating heat pipe made with AM-based polymers has proven to be advantageous in internal flow visualization, various flow optimization, and hybrid design with composite materials, offering a practical alternative for high-power electronic devices and aerospace thermal-management systems.

5. Radiation heat transfer for thermal management using AM

This section introduces cases related to the regulation of visible light and IR radiation using AM. In the case of visible light, it is responsible for the largest portion of energy within the solar spectrum. Solar radiation spans from UV (~200 nm) to near-IR (~2500 nm), with visible light alone accounting for about 43% of solar radiation, indicating its high energy content. Meanwhile, IR covers a very broad range from near-IR at 750 nm—which is included in sunlight—to far-IR at 1 mm. Significant portions of the IR spectrum are absorbed by gases such as carbon dioxide and water vapor.[135] Particularly, the broad band of mid-IR (5–8 μm) is quickly absorbed by the atmosphere, making it impractical for atmospheric applications. Therefore, the IR regions most commonly utilized in research are the near-IR (750–2500 nm), corresponding to solar radiation, and certain portions of Earth's radiation, especially the atmospheric window in the long-wavelength IR region (8–13 μm). The atmospheric window is crucial because it allows radiative heat to pass from the Earth's surface (~300 K) directly to outer space (~3 K) with minimal atmospheric reabsorption.[136] By controlling the emissivity of materials in the visible and IR regions, various metamaterials with added functionalities can be developed.[137] For example, high solar reflectance and efficient thermal emission through the atmospheric window are two key factors for achieving passive daytime radiative cooling[27] (Figure 9A). In addition, modulating IR emissivity enables IR stealth.

As with previous sections, the use of particles via DIW is a prominent approach. For instance, a multifunctional material (methyltrimethoxysilane/SiO_2/CNFs ink) has been reported, utilizing CNFs and silica nanoparticles to achieve porous lattice radiative cooling with a thermal conductivity as low as 0.05 W/(m·K).[138] Through AM, a radiative cooling structure was developed that effectively cools electronic devices under sunlight during the day. The fabricated structure lowered device temperatures by 6.16°C thanks to high solar reflectance and high IR emissivity, while also ensuring mechanical stability. In a similar example, an ink composed of polyethylene and SiO_2 particles was prepared and printed by DIW to cool buildings through solar reflection and IR emission passively[139] (Figure 9B). Using commercial polymer processing technologies such as molding, extrusion, and 3D printing, a low-cost, mass-producible nanoporous polymer matrix composite was produced, achieving 96.2% solar reflectance, over 90% IR emissivity, 6.1°C cooling under direct sunlight, and a net cooling power of 85 W/m^2. Another study developed a polymer aerogel-based radiative cooling structure by DIW-based AM, featuring a cross-linked network of polymethylsilsesquioxane and CNFs, followed by freeze-drying. This structure exhibited almost no volume shrinkage during freeze-drying and greatly improved interlayer interfaces, resulting in excellent fatigue resistance and environmental durability. The aerogel also demonstrated 94.2% solar reflectance, 95.6% atmospheric window emissivity, a cooling performance of 72.2 W/m^2, a cooling effect of 5.8°C, excellent insulation (0.034 W/[m·K]), and both water repellency and flame retardancy. Examples of radiative cooling material development using additive methods such as DIW and SLA can be found in applications ranging from fully uniform films[140] to multifunctional wearable smart sportswear,[141,142] and robot shells[143] (Figure 9C-E). In addition, there are cases where inks with tunable visible light emissivity are developed and used to fabricate colored radiative cooling films via DIW-based 3D printing.[14] For example, colored radiative cooling films have been produced using PVC/DMF inks, demonstrating the vast research possibilities enabled by the versatility of inks and their particle components (Figure 9F).

Meanwhile, there are also reported cases of IR stealth research aimed at drastically lowering IR emissivity (Figure 9G). The use of 3D-printed molds to create 3D aerogel structures has been reported for some time; a representative example is the development of a honeycomb-based lightweight aerogel composite for IR stealth, integrating reduced emissivity, heat absorption, and insulation functions[144] (Figure 9H). Using MXene, PVA, and PCMs, these composites were fabricated via 3D-printed molds, freeze-drying, and vacuum impregnation, resulting in low emissivity (0.273), high latent heat (105.3 J/g), and excellent mechanical strength. Even when exposed to a heat source at 100–120°C,the radiative temperature remained around 30°C, demonstrating effective IR stealth performance. More recent research has even used 3D printers to directly print IR stealth metamaterials; for

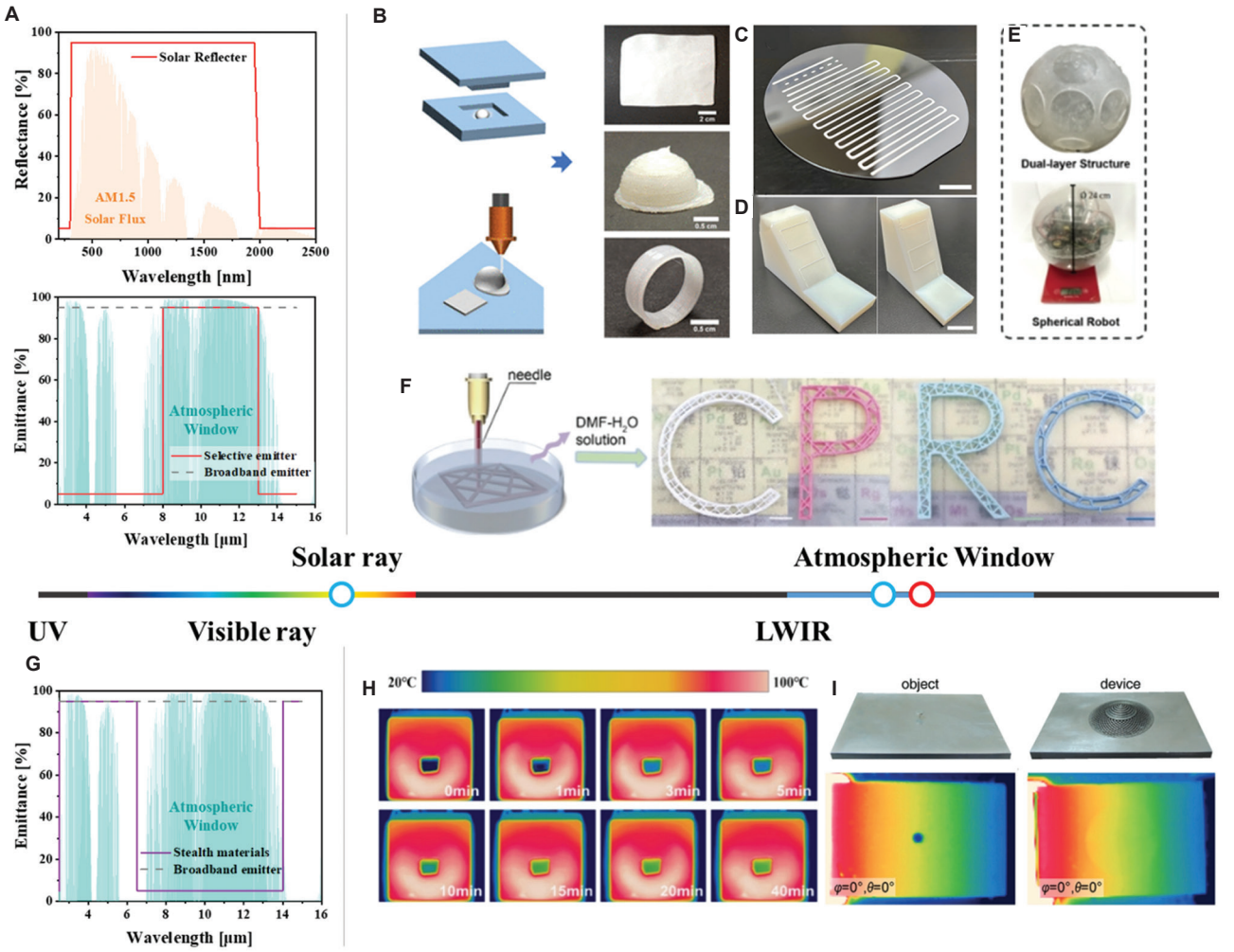

Figure 9. Working principles and representative examples of radiative thermal metamaterials based on additive manufacturing. (A) Conceptual graph illustrating selective emitters for solar reflection and IR emission to prevent radiative heat, such as radiative cooling. (B) 3D-printable nanoporous polymer matrix composites.[139] Copyright © 2021 American Chemical Society. Reproduced with permission of the American Chemical Society. (C and D) The 3D-printable polyvinylpyrrolidone-linked hollow silica nanoparticle.[140] (E) 3D-printed robot shell for daytime radiative cooling.[143] (F) PVC/DMF colored passive radiative coolers film.[14] Copyright © 2024 American Chemical Society. Reproduced with permission of the American Chemical Society. (G) Conceptual graph of IR emissivity for shielding against IR thermal radiation, such as IR stealth and thermal cloak. (H) Brick-like MXene@PVA/PCM composite aerogels with a honeycomb structure.[144] Copyright © 2024 American Chemical Society. Reproduced with permission of the American Chemical Society. (I) 3D meta-helmet for object camouflage.[16] Copyright © 2020 Wiley. Reproduced with permission of Wiley.
Abbreviations: DMF: *N*,*N*-Dimethylformamide; LWIR: Long-wave infrared; PCM: Phase change material; PVA: Polyvinyl alcohol; PVC: Polyvinyl chloride; UV: Ultraviolet.

example, an Al alloy helmet produced by L-PBF printing for IR camouflage has also been reported[16] (Figure 9I).

For this section, we have thoroughly reviewed the latest trends and application cases of AM technologies for controlling wavelength-selective radiative heat transfer in thermal metamaterials with structures ranging from the nanoscale to the macroscale. Depending on unit cell size and design requirements, a variety of AM processes, such as DIW and FFF, are selected. It has been confirmed that functional composites can be developed by precisely introducing metallic and ceramic particles into polymer matrices, enabling control over visible and IR light. For instance, porous structures fabricated from silica or cellulose nanofibers have demonstrated their effectiveness in a variety of applications, including radiative cooling achieved by high solar reflectance and IR emission. Recently, there have been consistent reports of advances such as aerogels with extremely low IR emissivity and 3D-printed helmets made from aluminum alloys, which simultaneously realize radiative heat concealment and IR stealth. In summary, AM

technologies drastically increase the freedom of shaping and structural design of thermal metamaterials and are a key solution for accurately implementing target properties in desired wavelength ranges by combining various functional particles. AM thus serves as a foundational technology that expands the boundaries of metamaterial applications, such as wavelength-selective radiation shielding, radiative cooling, and stealth, and is expected to play an increasingly important role in future thermal management and energy applications.

Furthermore, a recent study showed that a tubular ceramic lattice structure fabricated using SLA 3D printing can enhance radiative heat transfer by as much as 160–280% in high-temperature environments, while achieving low pressure drop and enabling efficient radiative heating of fluids within the structure.[145] This indicates that the convergence of radiative heat transfer and AM goes beyond the wavelength selectivity of the material itself, allowing for consideration of interactions with fluid flow. Such an integrated approach is expected to greatly contribute not only to broadening the potential for application in engineering devices such as heat exchangers but also to expanding the design freedom and application range of additive-manufactured radiative heat transfer materials.

6. Future perspectives

The continuous evolution of AM promises significant advancements in thermal management solutions across various sectors, including electronics, automotive, aerospace, and construction. Key future research directions can be categorized as follows:

(i) Advanced material development: Future research should focus on developing new composite materials with enhanced thermal properties. Combining high thermal conductivity materials, such as graphene and BN, with polymers through precise AM techniques will likely achieve unprecedented heat dissipation performance. In addition, integrating PCMs into complex AM structures may further revolutionize energy storage and temperature regulation systems.

(ii) Multifunctional metamaterials: Exploration into AM-enabled thermal metamaterials presents vast opportunities. The integration of thermal cloaking, thermal focusing, and directionally controlled heat transfer capabilities into single structures can open avenues for advanced thermal management applications in electronics cooling, building insulation, and stealth technologies. Further research into improving the mechanical robustness and scalability of these metamaterials is essential.

(iii) Optimization of computationally efficient thermal modeling tools using machine learning: There is great potential in combining AM with efficient computational thermal modeling tools such as topology optimization and machine learning algorithms. Enhanced predictive capabilities through AI will facilitate highly efficient and customized thermal management designs, significantly reducing design-to-product cycles. Developing standardized databases and predictive models for AM processes will streamline material selection and process parameter optimization.

(iv) Sustainability and scalability: Emphasis on environmentally friendly AM processes, recyclable materials, and waste reduction should be prioritized. Scaling AM technologies for mass production, particularly for large-scale thermal management solutions, is critical. Further development in high-throughput and cost-effective AM methods, such as VPP and MJ, will support broader adoption in industries.

(v) Hybrid and multimaterial printing: The future of AM thermal management will likely involve hybrid printing techniques combining multiple materials in a single process. This will enable functionally graded materials with tailored thermal, electrical, and mechanical properties, allowing for more integrated and complex thermal management solutions.

(vi) Reducing thermal interfacial resistance in multimaterial AM parts: Thermal interfacial resistance is essential for effective heat transfer. Interfaces between dissimilar materials often cause phonon scattering and weak bonding, increasing thermal resistance. Strategies such as functionally graded interfaces, optimized printing parameters, and surface treatments help improve interfacial thermal conductance. These approaches enhance both thermal performance and structural reliability in AM-based thermal management systems.

(vii) Designing lattice structures with validated thermo-mechanical performance cycling: Lattice structures are increasingly used in thermal management due to their lightweight and high surface area, which enhances heat dissipation and structural efficiency. However, repeated thermal and mechanical stresses can degrade their performance over time. To address this, researchers combine simulation and experimental methods to optimize geometry, material combinations, and structural density. This ensures stable thermal and mechanical performance even under long-term operational conditions.

7. Conclusion

Developments in the AM technology have significantly advanced thermal management, providing unparalleled

opportunities in design freedom, material customization, and performance optimization across conductive, convective, boiling, and radiative heat transfer applications. By enabling intricate internal geometries and precise material placement, AM facilitates the development of tailored thermal solutions such as advanced heat exchangers, sophisticated thermal metamaterials, and integrated two-phase cooling devices. Enhanced thermal conductivity through polymer composites and optimized microchannel and TPMS structures highlight AM's potential to meet escalating heat dissipation demands, particularly in electronics and high-power devices. Moreover, AM's ability to integrate PCMs and functionally graded materials allows for highly efficient thermal regulation, energy storage, and advanced thermal cloaking functionalities. Despite these promising advancements, significant challenges remain, including ensuring structural integrity, precise microstructural control, and scalable, cost-effective manufacturing processes. Addressing these issues through continued research and integration with computational methods like topology optimization and AI-driven design will be crucial.

Looking forward, hybrid and multimaterial AM techniques hold immense promise in overcoming current limitations, paving the way for multifunctional metamaterials and highly customizable thermal management solutions. As AM technologies continue to mature, their integration into broader engineering sectors will drive substantial improvements in energy efficiency, sustainability, and system reliability. Future advancements will likely focus on overcoming technical barriers associated with scaling production, ensuring repeatability, and developing standardized AM processes. Moreover, extensive exploration into recyclable and environmentally sustainable materials will be vital in aligning AM practices with global sustainability goals. Enhanced collaboration between academia, industry, and regulatory bodies will further accelerate AM innovations, ensuring rapid and effective implementation in practical scenarios. Ultimately, AM stands to significantly enhance future thermal management strategies, supporting innovative advancements in diverse industrial applications.

Acknowledgments

None.

Funding

This work was supported by an Agency for Defense Development of Korea (ADD) grant (915050201), National Research Foundation of Korea (NRF) funded by the Korean government (Ministry of Science and ICT) (2023R1A2C2006407, 2020R1A5A1018153), and Korea Evaluation Institute of Industrial Technology (KEIT) grant funded by the Korea government (MOTIE) (No. RS-2024-00433288).

Conflict of interest

Wonjoon Choi is an Editorial Board Member of this journal, but was not in any way involved in the editorial and peer-review process conducted for this paper, directly or indirectly. Separately, other authors declared that they have no known competing financial interests or personal relationships that could have influenced the work reported in this paper.

Author contributions

Conceptualization: Jaemin Lee, Wonjoon Choi
Writing–original draft: All authors
Writing–review & editing: Jaemin Lee, Wonjoon Choi

Ethics approval and consent to participate

Not applicable.

Consent for publication

Not applicable.

Availability of data

Not applicable.

References

1. Hamilton I, Kennard H, Rapf O, *et al. Global Status Report for Buildings and Construction-Beyond Foundations: Mainstreaming Sustainable Solutions to Cut Emissions from the Buildings Sector*; 2024.

2. Hwang FS, Confrey T, Reidy C, *et al*. Review of battery thermal management systems in electric vehicles. *Renew Sustain Energy Rev*. 2024;192:114171.

   doi: 10.1016/j.rser.2023.114171

3. Rakshith BL, Asirvatham LG, Angeline AA, *et al.* Cooling of high heat flux miniaturized electronic devices using thermal ground plane: An overview. *Renew Sustain Energy Rev*. 2022;170:112956.

   doi: 10.1016/j.rser.2022.112956

4. Nair V, Baby A, Anoop MB, Indrajith S, Murali M, Nair MB. A comprehensive review of air-cooled heat sinks for thermal management of electronic devices. *Int Commun Heat Mass Transfer*. 2024;159:108055.

   doi: 10.1016/j.icheatmasstransfer.2024.108055

5. Careri F, Khan RHU, Todd C, Attallah MM. Additive manufacturing of heat exchangers in aerospace applications: A review. *Appl Thermal Eng*. 2023;235:121387.

doi: 10.1016/j.applthermaleng.2023.121387

6. Khan N, Riccio A. A systematic review of design for additive manufacturing of aerospace lattice structures: Current trends and future directions. *Prog Aerospace Sci*. 2024;149:101021.

   doi: 10.1016/j.paerosci.2024.101021

7. Lim DD, Lee J, Park J, Choi W. High-resolution and electrically conductive three-dimensional printing of carbon nanotube-based polymer composites enabled by solution intercalation. *Carbon*. 2022;194:1-9.

8. Yadav S, Liu S, Singh RK, Sharma AK, Rawat P. A state-of-art review on functionally graded materials (FGMs) manufactured by 3D printing techniques: Advantages, existing challenges, and future scope. *J Manuf Processes*. 2024;131:2051-2072.

   doi: 10.1016/j.jmapro.2024.10.026

9. Lim DD, Park J, Lee J, *et al.* Broadband mechanical metamaterial absorber enabled by fused filament fabrication 3D printing. *Addit Manuf*. 2022;55:102856.

   doi: 10.1016/j.addma.2022.102856

10. Kruzel M, Dutkowski K, Bohdal T, Litwin A, Sawicki J, Kępa E. A new approach for heat transfer coefficient determination in triply periodic minimal surface-based heat exchangers. *Int Commun Heat Mass Transfer*. 2024;157:107778.

    doi: 10.1016/j.icheatmasstransfer.2024.107778

11. Tang W, Zou C, Zhou H, *et al*. A novel convective heat transfer enhancement method based on precise control of gyroid-type TPMS lattice structure. *Appl Thermal Eng*. 2023;230:120797.

    doi: 10.1016/j.applthermaleng.2023.120797

12. Chandra S, Wang C, Tor SB, Ramamurty U, Tan X. Powder-size driven facile microstructure control in powder-fusion metal additive manufacturing processes. *Nat Commun*. 2024;15(1):3094.

    doi: 10.1038/s41467-024-47257-w

13. Ghasemi A, Fereiduni E, Elbestawi M, *et al.* Influence of the graphene incorporation on nanostructure and thermal properties of the laser powder bed fusion processed AlSi12 matrix composites. *J Alloys Compds*. 2025;1010:177075.

    doi: 10.1016/j.jallcom.2024.177075

14. Lin Y, Qin C, Fang L, Wang J, Li D. Colored polymeric films with a bilayer porous design for efficient subambient radiative cooling. *ACS Appl Polym Mater*. 2024;6(1):722-731.

    doi: 10.1021/acsapm.3c02318

15. Oh SH, An CH, Seo B, Kim J, Park CY, Park K. Functional morphology change of TPMS structures for design and additive manufacturing of compact heat exchangers. *Addit Manuf*. 2023;76:103778.

    doi: 10.1016/j.addma.2023.103778

16. Peng YG, Li Y, Cao PC, Zhu XF, Qiu CW. 3D printed meta-helmet for wide-angle thermal camouflages. *Adv Funct Mater*. 2020;30(28):2002061.

    doi: 10.1002/adfm.202002061

17. Ahmad MJ, Tian X, Dai X, *et al.* Non-conformal thermal cloak metamaterial by continuous metal fiber embedded 3D printing. *Int J Heat Mass Transfer*. 2025;242:126796.

    doi: 10.1016/j.ijheatmasstransfer.2025.126796

18. ISO/ASTM 52900. *Additive Manufacturing-General Principles - Fundamentals and Vocabulary*. United States: ISO/ASTM; 2021.

19. Xiao Z, Chen C, Zhu H, *et al.* Study of residual stress in selective laser melting of Ti6Al4V. *Mater Design*. 2020;193:108846.

    doi: 10.1016/j.matdes.2020.108846

20. Panwisawas C, Gong Y, Tang YT, Reed RC, Shinjo J. Additive manufacturability of superalloys: Process-induced porosity, cooling rate and metal vapour. *Addit Manuf*. 2021;47:102339.

    doi: 10.1016/j.addma.2021.102339

21. Foteinopoulos P, Papacharalampopoulos A, Stavropoulos P. Additive manufacturing simulations: An approach based on space partitioning and dynamic 3D mesh adaptation. *Addit Manuf Lett*. 2024;11:100256.

    doi: 10.1016/j.addlet.2024.100256

22. Jiong S, Yun J, Lee J, *et al*. Nanosized boron nitride-incorporated polyvinyl alcohol composites with TEMPO-oxidized cellulose nanofibers as ultrathin thermal interface materials. *Chem Eng J*. 2024;500:157243.

23. Yun J, Lee J, Kim J, Lee J, Choi W. Hexagonal boron nitride nanosheets/graphene nanoplatelets/cellulose nanofibers-based multifunctional thermal interface materials enabling electromagnetic interference shielding and electrical insulation. *Carbon*. 2024;228:119397.

24. Hu H, Xu C, Zhao Y, Ziegler KJ, Chung JN. Boiling and quenching heat transfer advancement by nanoscale surface modification. *Sci Rep*. 2017;7(1):6117.

    doi: 10.1038/s41598-017-06050-0

25. Lee J, Kyeong D, Kim J, Choi W. Layer-by-layer self-assembled functional coatings of carbon nanotube-polyethylenimine for enhanced heat transfer of heat sinks. *Int J Heat Mass Transfer*. 2022;184:122344.

    doi: 10.1016/j.ijheatmasstransfer.2021.122344

26. Lee J, Kim J, Seo B, Shin D, Hwang S, Choi W. Layer-by-layer solution-processed two-dimensional graphene oxide-polyethylenimine thin-film coatings for enhanced pool boiling heat transfer. *Int J Heat Mass Transfer*. 2023;209:124067.

27. Hossain MM, Gu M. Radiative cooling: Principles, progress, and potentials. *Adv Sci*. 2016;3(7):1500360.

doi: 10.1002/advs.201500360

28. Radhakrishnan M, Sharma S, Palaniappan S, *et al*. Influence of thermal conductivity on evolution of grain morphology during laser-based directed energy deposition of CoCrxFeNi high entropy alloys. *Addit Manuf*. 2024;92:104387.

doi: 10.1016/j.addma.2024.104387

29. Lin K, Tian H, Gu D, Wang C, Yuan L, Sun J. Laser powder bed fusion of Cu–Al–Ni–Mn shape-memory alloy for the application of active heat sinks: Processability, microstructures, and shape-memory effect. *Adv Eng Mater*. 2024;26(4):2301224.

doi: 10.1002/adem.202301224

30. Fereiduni E, Ghasemi A, Sargent N, *et al*. Synergy of laser powder bed fusion (LPBF) and heat treatment for CuNi2SiCr alloy enhancement. *Mater Design*. 2025;255:114189.

doi: 10.1016/j.matdes.2025.114189

31. Gao J, Hao M, Wang Y, *et al*. 3D printing boron nitride nanosheets filled thermoplastic polyurethane composites with enhanced mechanical and thermal conductive properties. *Addit Manuf*. 2022;56:102897.

doi: 10.1016/j.addma.2022.102897

32. Zhang C, Deng K, Li X, Fu KK, Ni C. Thermally conductive 3D-printed carbon-nanotube-filled polymer nanocomposites for scalable thermal management. *ACS Appl Nano Mater*. 2023;6(14):13400-13408.

doi: 10.1021/acsanm.3c02067

33. Olcun S, Ibrahim Y, Isaacs C, Karam M, Elkholy A, Kempers R. Thermal conductivity of 3D-printed continuous pitch carbon fiber composites. *Addit Manuf Lett*. 2023;4:100106.

doi: 10.1016/j.addlet.2022.100106

34. Cai Z, Zhang J, Zhang L, *et al*. Fluid-assisted fused deposition modeling 3D printing of anisotropically thermally conductive polymer composites with precisely tunable heat transfer pathways. *Compos Commun*. 2024;46:101835.

doi: 10.1016/j.coco.2024.101835

35. Guo Y, Wang S, Zhang H, *et al*. Consistent thermal conductivities of spring-like structured polydimethylsiloxane composites under large deformation. *Adv Mater*. 2024;36(39):2404648.

doi: 10.1002/adma.202404648

36. Hou L, Ji JC, Cui GP, *et al*. 3D printable phase change based thermal interface material with lower total thermal resistance at operating temperature. *J Energy Storage*. 2024;99:113303.

doi: 10.1016/j.est.2024.113303

37. Fang B, Zhang G, Zou F, *et al*. 3D printing interconnected segregated composites to simultaneously enhance thermal conductivity and mechanical properties. *ACS Appl Polym Mater*. 2024;6(8):4904-4911.

doi: 10.1021/acsapm.4c00654

38. Peng Z, Lv Q, Jing J, Pei H, Chen Y, Ivanov E. FDM-3D printing LLDPE/BN@GNPs composites with double network structures for high-efficiency thermal conductivity and electromagnetic interference shielding. *Compos Part B Eng*. 2023;251:110491.

doi: 10.1016/j.compositesb.2022.110491

39. Kang Z, Xi M, Li N, Zhang S, Wang Z. Anisotropic thermal conductivity of 3D printed graphene enhanced thermoplastic polyurethanes structure toward photothermal conversion. *Carbon*. 2025;234:120023.

doi: 10.1016/j.carbon.2025.120023

40. Xia R, Zhu S, Zhen F, *et al*. Vertical 3D printing of rGO/CNTs arrays for thermal interface materials with *in-situ* local temperature monitoring function. *Chem Eng J*. 2024;496:153643.

doi: 10.1016/j.cej.2024.153643

41. Qiu L, Wang X, Feng G, Feng Y. Tailorable thermal conduction and thermal energy storage behaviors in 3D printed hierarchical cellular structure-based phase change materials. *Small Methods*. 2025;9:2402089.

doi: 10.1002/smtd.202402089

42. Taleb O, Jutkofsky M, Measel R, *et al*. Thermal conductivity of 3D-printed block-copolymer-inspired structures. *Int J Heat Mass Transfer*. 2024;235:126186.

doi: 10.1016/j.ijheatmasstransfer.2024.126186

43. Wang L, Feng J, Luo Y, *et al*. Three-dimensional-printed silica aerogels for thermal insulation by directly writing temperature-induced solidifiable inks. *ACS Appl Mater Interfaces*. 2021;13(34):40964-40975.

doi: 10.1021/acsami.1c12020

44. Zhu T, Ren Z, Wang D, *et al*. Reactive 3D printed silanized cellulose nanofiber aerogels for solar-thermal regulatory cooling. *Compos Part A Appl Sci Manuf*. 2025;192:108761.

doi: 10.1016/j.compositesa.2025.108761

45. Liu C, Li MC, Liu X, Zhou G, Liu C, Mei C. 3D printing of customized lignocellulose nanofibril aerogels for efficient thermal insulation. *Addit Manuf*. 2023;78:103841.

doi: 10.1016/j.addma.2023.103841

46. Fu Z, Yu D, Xue T, Zhang X, Fan W. 3D printed polyimide-based composite aerogels with shape memory and thermal insulation properties. *Compos Commun*. 2025;56:102335.

doi: 10.1016/j.coco.2025.102335

47. Pei Y, Shen Z, Zhou J, Yang B. Experimental and theoretical thermal performance analysis of additively manufactured polymer vacuum insulation panels. *Appl Thermal Eng*. 2024;256:123957.

doi: 10.1016/j.applthermaleng.2024.123957

48. Sha W, Xiao M, Zhang J, *et al*. Robustly printable freeform thermal metamaterials. *Nat Commun*. 2021;12(1):7228.

doi: 10.1038/s41467-021-27543-7

49. Rao Y, Yan Y, Mei H, *et al*. 3D-printed lattice structures with SiC whiskers to strengthen thermal metamaterials. *Ceramics Int*. 2022;48(21):32283-32289.

doi: 10.1016/j.ceramint.2022.07.170

50. Freeman TB, Foster KEO, Troxler CJ, *et al*. Advanced materials and additive manufacturing for phase change thermal energy storage and management: A review. *Adv Energy Mater*. 2023;13(24):2204208.

doi: 10.1002/aenm.202204208

51. Yu D, Chi G, Mao X, *et al*. Volume-metallization 3D-printed polymer composites. *Adv Mater*. 2024;36(35):2403088.

doi: 10.1002/adma.202403088

52. Lee J, Han H, Noh D, *et al*. Multiscale porous architecture consisting of graphene aerogels and metastructures enabling robust thermal and mechanical functionalities of phase change materials. *Adv Funct Mater*. 2024;34(42):2405625.

53. Song C, Lee J, Lim DD, Choi W. Rationally tunable phase change material thermal properties enabled by three-dimensionally printed structural materials and carbon-based functional additives. *Int J Energy Res*. 2023;2023(1):6658082.

54. Liu C, Liu X, Shi X, *et al*. 3D printing of phase change material-based Pickering emulsion gel for solar-thermal-electric conversion. *Chem Eng J*. 2024;499:155940.

doi: 10.1016/j.cej.2024.155940

55. Er Y, Güler O, Hekimoğlu G, *et al*. Thermophysical properties and solar thermal energy storage performance of phase change composites manufactured by vat photopolymerization 3D printing technique. *J Energy Storage*. 2023;73:109124.

doi: 10.1016/j.est.2023.109124

56. Er Y, Güler O, Ustaoğlu A, *et al*. Characterisation and energy storage performance of 3D printed-photocurable resin/microencapsulated phase change material composite. *Thermal Sci Eng Prog*. 2024;48:102381.

doi: 10.1016/j.tsep.2023.102381

57. Bender J, Dubil K, Korn F, Wetzel T, Dietrich B. Modelling of heat transfer and pressure drop during flow boiling of CO_2 in a horizontal tube with periodic open cellular inserts. *Chem Eng Process Process Intensification*. 2024;203:109891.

doi: 10.1016/j.cep.2024.109891

58. Righetti G, Savio G, Meneghello R, Doretti L, Mancin S. Experimental study of phase change material (PCM) embedded in 3D periodic structures realized via additive manufacturing. *Int J Thermal Sci*. 2020;153:106376.

doi: 10.1016/j.ijthermalsci.2020.106376

59. Diani A, Nonino C, Rossetto L. Melting of phase change materials inside periodic cellular structures fabricated by additive manufacturing: Experimental results and numerical simulations. *Appl Thermal Eng*. 2022;215:118969.

doi: 10.1016/j.applthermaleng.2022.118969

60. Wang C, Liu C, Li C. Additive manufacturing of shape-stabilized composite phase change materials via ultraviolet curing. *Addit Manuf*. 2023;61:103341.

doi: 10.1016/j.addma.2022.103341

61. Piacquadio S, Schirp-Schoenen M, Mameli M, Filippeschi S, Schröder KU. Experimental analysis of the thermal energy storage potential of a phase change material embedded in additively manufactured lattice structures. *Appl Thermal Eng*. 2022;216:119091.

doi: 10.1016/j.applthermaleng.2022.119091

62. Kim J, Lee J, Song C, Yun J, Choi W. Enhanced thermal performances of PCM heat sinks enabled by layer-by-layer-assembled carbon nanotube–polyethylenimine functional interfaces. *Energy Convers Manage*. 2022;266:115853.

63. Shamvedi D, Mccarthy OJ, Eoghan OD, Cyril D, Paul OL, Raghavendra R. 3D Metal printed heat sinks with longitudinally varying lattice structure sizes using direct metal laser sintering. *Virtual Phys Prototyp.* 2018;13(4):301-310.

doi: 10.1080/17452759.2018.1479528

64. Lorenzon A, Vaglio E, Casarsa L, Totis G. Effects of different cross-sections of body centered cubic cells on pressure drop and heat transfer of additively manufactured heat sinks. *Int J Heat Mass Transfer*. 2024;222:125170.

doi: 10.1016/j.ijheatmasstransfer.2024.125170

65. Tseng PH, Tsai KT, Chen AL, Wang CC. Performance of novel liquid-cooled porous heat sink via 3-D laser additive manufacturing. *Int J Heat Mass Transfer*. 2019;137:558-564.

doi: 10.1016/j.ijheatmasstransfer.2019.03.116

66. Lazarov BS, Sigmund O, Meyer KE, Alexandersen J. Experimental validation of additively manufactured optimized shapes for passive cooling. *Appl Energy*. 2018;226:330-339.

doi: 10.1016/j.apenergy.2018.05.106

67. Ho TYK, Ng AYR, Ye P, *et al*. Realization of vat photopolymerisation of dense SiC ceramics with SiO2/MgSO4 coated sub-micron powders for efficient heat dissipation. *Addit Manuf*. 2023;73:103664.

doi: 10.1016/j.addma.2023.103664

68. Sheng P, Nie G, Li Y, *et al*. Enhanced curing behavior, mechanical and thermal properties of 3D printed aluminum nitride ceramics using a powder coating strategy. *Addit Manuf*. 2023;74:103732.

doi: 10.1016/j.addma.2023.103732

69. Song C, Lee J, Seo B, Shim JH, Hu R, Choi W. Enhanced cooling performance of three-dimensional printed heat sink via solution-processed layer-by-layer CNT coatings. *Adv Eng Mater*. 2023;25(20):2300669.

70. Huttunen E, Nykänen MT, Alexandersen J. Material extrusion additive manufacturing and experimental testing of topology-optimised passive heat sinks using a thermally-conductive plastic filament. *Addit Manuf*. 2022;59:103123.

doi: 10.1016/j.addma.2022.103123

71. Timbs K, Khatamifar M, Antunes E, Lin W. Experimental study on the heat dissipation performance of straight and oblique fin heat sinks made of thermal conductive composite polymers. *Thermal Sci Eng Prog*. 2021;22:100848.

doi: 10.1016/j.tsep.2021.100848

72. Ventola L, Robotti F, Dialameh M, *et al*. Rough surfaces with enhanced heat transfer for electronics cooling by direct metal laser sintering. *Int J Heat Mass Transfer*. 2014;75:58-74.

doi: 10.1016/j.ijheatmasstransfer.2014.03.037

73. Kirsch KL, Thole KA. Pressure loss and heat transfer performance for additively and conventionally manufactured pin fin arrays. *Int J Heat Mass Transfer*. 2017;108:2502-2513.

doi: 10.1016/j.ijheatmasstransfer.2017.01.095

74. Collins IL, Weibel JA, Pan L, Garimella SV. A permeable-membrane microchannel heat sink made by additive manufacturing. *Int J Heat Mass Transfer*. 2019;131:1174-1183.

doi: 10.1016/j.ijheatmasstransfer.2018.11.126

75. Kempers R, Colenbrander J, Tan W, Chen R, Robinson AJ. Experimental characterization of a hybrid impinging microjet-microchannel heat sink fabricated using high-volume metal additive manufacturing. *Int J Thermofluids*. 2020;5-6:100029.

doi: 10.1016/j.ijft.2020.100029

76. Xu C, Xu S, Wang Z, Feng D. Experimental investigation of flow and heat transfer characteristics of pulsating flows driven by wave signals in a microchannel heat sink. *Int Commun Heat Mass Transfer*. 2021;125:105343.

doi: 10.1016/j.icheatmasstransfer.2021.105343

77. Santos S, Matos C, Duarte I, Olhero S, Miranda G. Effect of TPMS reinforcement on the mechanical properties of aluminium–alumina interpenetrating phase composites. *Prog Addit Manuf*. 2025;10(2):1187-1199.

78. Yan K, Deng H, Xiao Y, Wang J, Luo Y, Yan J. Influence of polishing process on surface morphology and thermo-hydraulic performance of additively manufactured Gyroid-structured heat exchanger. *Appl Thermal Eng*. 2024;253:123828.

doi: 10.1016/j.applthermaleng.2024.123828

79. Raafat A, Alteneiji M, Kamra M, Al Nuaimi S. Hydrothermal performance of microchannel heat sink integrating pin fins based on triply periodic minimal surfaces. *Case Stud Thermal Eng*. 2025;66:105773.

doi: 10.1016/j.csite.2025.105773

80. Ning J, Wang X, Sun Y, *et al*. Experimental and numerical investigation of additively manufactured novel compact plate-fin heat exchanger. *Int J Heat Mass Transfer*. 2022;190:122818.

doi: 10.1016/j.ijheatmasstransfer.2022.122818

81. Ozguc S, Pan L, Weibel JA. Optimization of permeable membrane microchannel heat sinks for additive manufacturing. *Appl Thermal Eng*. 2021;198:117490.

doi: 10.1016/j.applthermaleng.2021.117490

82. Kong D, Jung E, Kim Y, *et al*. An additively manufactured manifold-microchannel heat sink for high-heat flux cooling. *Int J Mechan Sci*. 2023;248:108228.

doi: 10.1016/j.ijmecsci.2023.108228

83. Bacellar D, Aute V, Huang Z, Radermacher R. Design optimization and validation of high-performance heat exchangers using approximation assisted optimization and additive manufacturing. *Sci Technol Built Environ*. 2017;23(6):896-911.

doi: 10.1080/23744731.2017.1333877

84. Liu C, Zhang M, Bi G, *et al*. Research on comprehensive heat dissipation characteristics of AlSi7Mg TPMS heat sinks manufactured by laser powder bed fusion. *Appl Thermal Eng*. 2025;261:124941.

doi: 10.1016/j.applthermaleng.2024.124941

85. Tan H, Wu L, Wang M, Yang Z, Du P. Heat transfer improvement in microchannel heat sink by topology design and optimization for high heat flux chip cooling. *Int J Heat Mass Transfer*. 2019;129:681-689.

doi: 10.1016/j.ijheatmasstransfer.2018.09.092

86. Ozguc S, Teague TFG, Pan L, Weibel JA. Experimental study of topology optimized, additively manufactured microchannel heat sinks designed using a homogenization approach. *Int J Heat Mass Transfer*. 2023;209:124108.

doi: 10.1016/j.ijheatmasstransfer.2023.124108

87. Orakwe JN, Shahabad SI, Ibhadode O, Bonakdar A, Toyserkani E. An integration of topology optimization and conformal minimal surfaces for additively manufactured liquid-cooled heat sinks. *Addit Manuf*. 2025;107:104814.

doi: 10.1016/j.addma.2025.104814

88. Han XH, Liu HL, Xie G, Sang L, Zhou J. Topology optimization for spider web heat sinks for electronic cooling. *Appl Thermal Eng*. 2021;195:117154.

doi: 10.1016/j.applthermaleng.2021.117154

89. Robertson J, Carter E, Thompson M, White S. Multi-objective design of heat sink fins for thermal efficiency and

manufacturability. *Int J Eng Adv*. 2025;2(1):32-39.

doi: 10.71222/1aqrg398

90. Wang W, Zhu H, Zhang W, Xiao Z. A high heat transfer performance of inclined rib mini-channel heat sink designed by machine learning and laser powder bed fusion. *Phys Fluids*. 2025;37(1):012009.

doi: 10.1063/5.0247582

91. Wang W, Zhang W, Yang X, Zhang B, Zhu H. Performance optimization of discrete sidewall features mini-channel heat sinks via laser powder bed fusion and machine learning. *Phys Fluids*. 2025;37(5):052002.

doi: 10.1063/5.0270757

92. Aksoy B, Salman OKM, Özsoy K. The estimation of the thermal performance of heat sinks manufactured by direct metal laser sintering based on machine learning. *Measurement*. 2024;225:113625.

doi: 10.1016/j.measurement.2023.113625

93. Thakur S, Talla G, Verma P. Residual stress, distortion, and porosity analysis of LED heat sink printed by SLM process using machine learning. *Eng Res Express*. 2021;3(4):045043.

doi: 10.1088/2631-8695/ac3dc6

94. Yeranee K, Rao Y. A review of recent investigations on flow and heat transfer enhancement in cooling channels embedded with triply periodic minimal surfaces (TPMS). *Energies*. 2022;15(23):8994.

95. Isenhart CR, Hayes AC, Whiting GL. Additive manufacturing of scalable jet impingement and radial taper enhancements for improved flow boiling performance. *Appl Therm Eng*. 2024;249:123355.

doi: 10.1016/j.applthermaleng.2024.123355

96. Liu H, Wang J, Gu Z, Fei X, Zhang L. Enhancement of pool boiling heat transfer using 3D-printed groove structure. *Int J Heat Mass Transfer*. 2022;183:122155.

doi: 10.1016/j.ijheatmasstransfer.2021.122155

97. Shim DI, Yun M, Kim YH, Lee D, Cho HH. 3D-Printed vapor guiding structures for enhanced pool boiling heat transfer. *Int J Mechan Sci*. 2025;286:109865.

doi: 10.1016/j.ijmecsci.2024.109865

98. Okwiri LA, Mochizuki T, Koito K, Fukui N, Enoki K. Enhanced pool boiling via binder-jetting 3D-printed porous copper structures: CHF and HTC investigation. *Appl Sci*. 2025;15(14):7892.

99. Lum LYX, Liu P, Ye H, Ho JY. Revealing microstructured surface critical heat flux degradation mechanisms and synergistic pool boiling enhancement in fluorinated fluids. *ACS Appl Mater Interfaces*. 2025;17(18):27331-27350.

doi: 10.1021/acsami.4c22543

100. Pi G, Deng D, Chen L, Xu X, Zhao C. Pool boiling performance of 3D-printed reentrant microchannels structures. *Int J Heat Mass Transfer*. 2020;156:119920.

doi: 10.1016/j.ijheatmasstransfer.2020.119920

101. Hayes A, Raghupathi PA, Emery TS, Kandlikar SG. Regulating flow of vapor to enhance pool boiling. *Appl Thermal Eng*. 2019;149:1044-1051.

doi: 10.1016/j.applthermaleng.2018.12.091

102. Shvetsov DA, Zhukov VI, Pavlenko AN. Heat transfer enhancement during boiling in horizontal layers of HFE-7100 on 2D modulated capillary-porous coatings. *Appl Thermal Eng*. 2025;263:125344.

doi: 10.1016/j.applthermaleng.2024.125344

103. Lee S, Yun S, Kwon J, Baek C, Lee D, Kim Y. Experimental investigation on boiling heat transfer performance of fractal microchannels for high heat dissipation applications. *Case Stud Thermal Eng*. 2023;52:103754.

doi: 10.1016/j.csite.2023.103754

104. Hasan M, Perna R, Elkholy A, Durfee J, Kempers R. A lightweight additively manufactured two-phase integrated natural convection heat sink. *Appl Thermal Eng*. 2025;266:125700.

doi: 10.1016/j.applthermaleng.2025.125700

105. Liu H, Gu Z, Liang J. Study on boiling heat transfer characteristics of composite porous structure fabricated by selective laser melting. *Materials*. 2023;16(19):6391.

106. Lum LYX, Leong KC, Ho JY. Optimizing additively manufactured macro-fin structure designs for enhanced pool boiling of dielectric fluids. *Int J Heat Mass Transfer*. 2024;219:124883.

doi: 10.1016/j.ijheatmasstransfer.2023.124883

107. Rozati SA, Gupta A. Enhanced phase change heat transfer with fused deposition modeling (FDM) printed pit and pillar (Pi2) arrays. *Exp Thermal Fluid Sci*. 2025;161:111337.

doi: 10.1016/j.expthermflusci.2024.111337

108. Lum LYX, Liu P, Ho JY. Micro/nanostructuring of metal additively manufactured aluminum alloy for enhanced pool boiling of dielectric fluids. *Int J Heat Mass Transfer*. 2024;221:125090.

doi: 10.1016/j.ijheatmasstransfer.2023.125090

109. Elkholy A, Kempers R. Enhancement of pool boiling heat transfer using 3D-printed polymer fixtures. *Exp Thermal Fluid Sci*. 2020;114:110056.

doi: 10.1016/j.expthermflusci.2020.110056

110. Ozguc S, Pan L, Weibel JA. An approach for topology optimization of heat sinks for two-phase flow boiling: Part 2 – Model calibration and experimental validation. *Appl Thermal Eng*. 2024;249:123338.

doi: 10.1016/j.applthermaleng.2024.123338

111. Zhou J, Yin Z. An experimental investigation on the flow boiling heat transfer performance of nanofluid in 3D printing minichannel heat sinks: A comparative study. *Nanomaterials* (*Basel*). 2025;15(14):1054.

doi: 10.3390/nano15141054

112. Kneer A, Wirtz M, Bozkurt MC, *et al.* One-piece stainless-steel 3D printed minichannel evaporators using flow boiling carbon dioxide. *Chem Eng Technol*. 2020;43(5):923-932.

doi: 10.1002/ceat.202000069

113. Wong KK, Leong KC. Nucleate flow boiling enhancement on engineered three-dimensional porous metallic structures in FC-72. *Appl Thermal Eng*. 2019;159:113846.

doi: 10.1016/j.applthermaleng.2019.113846

114. Silvi LD, Shanmugam AR, Park KS. Numerical study of pool boiling heat transfer on pin-fin surface submerged in dielectric fluid. *Thermal Sci Eng Prog*. 2025;61:103507.

doi: 10.1016/j.tsep.2025.103507

115. Zhou J, Li Q, Chen X. Micro pin fins with topologically optimized configurations enhance flow boiling heat transfer in manifold microchannel heat sinks. *Int J Heat Mass Transfer*. 2023;206:123956.

doi: 10.1016/j.ijheatmasstransfer.2023.123956

116. Zhou J, Zhou F, Zhao Q, Lu M, Li Q, Chen X. Flow boiling heat transfer in manifold microchannels with topologically optimized configurations. *Int Commun Heat Mass Transfer*. 2025;161:108555.

doi: 10.1016/j.icheatmasstransfer.2024.108555

117. Septet C, El Achkar G, Le Metayer O, Hugo JM. Experimental investigation of two-phase liquid-vapor flows in additive manufactured heat exchanger. *Appl Thermal Eng*. 2020;179:115638.

doi: 10.1016/j.applthermaleng.2020.115638

118. El Achkar G, Septet C, Le Metayer O, Hugo JM. Experimental thermohydraulic characterisation of flow boiling and condensation in additive manufactured plate-fin heat exchanger. *Int J Heat Mass Transfer*. 2022;199:123465.

doi: 10.1016/j.ijheatmasstransfer.2022.123465

119. Ye H, Lum LYX, Kandasamy R, Zhao H, Ho JY. Flow boiling heat transfer enhancement of R134a in additively manufactured minichannels with microengineered surfaces. *Appl Thermal Eng*. 2024;256:124150.

doi: 10.1016/j.applthermaleng.2024.124150

120. Akizuki Y, Odagiri K, Sawada K, Yoshizaki H, Sairaiji M, Ogawa H. Heat transport characterization on different orientations of a loop heat pipe with an additive manufactured evaporator. *Appl Thermal Eng*. 2025;264:125455.

doi: 10.1016/j.applthermaleng.2025.125455

121. Kappe K, Bihler M, Morawietz K, Hügenell PPC, Pfaff A, Hoschke K. Design concepts and performance characterization of heat pipe wick structures by LPBF additive manufacturing. *Materials*. 2022;15(24):8930.

122. Mezghani A, Dickman CJ, Reutzel EW, Nassar AR, Wolfe DE. Additively manufactured inconel 718 vapor chamber with conformal micro-pillar wicks: A low temperature concept demonstration. *Int J Heat Mass Transfer*. 2025;246:127056.

doi: 10.1016/j.ijheatmasstransfer.2025.127056

123. Robinson AJ, Colenbrander J, Deaville T, Durfee J, Kempers R. A wicked heat pipe fabricated using metal additive manufacturing. *Int J Thermofluids*. 2021;12:100117.

doi: 10.1016/j.ijft.2021.100117

124. Jafari D, Wits WW, Geurts BJ. Phase change heat transfer characteristics of an additively manufactured wick for heat pipe applications. *Appl Thermal Eng*. 2020;168:114890.

doi: 10.1016/j.applthermaleng.2019.114890

125. Meng X, Tan S, Yuan Z, Zhang Y, Chen L. Experimental study on the heat transfer performance of a vapour chamber with porous wick structures printed via metallic additive manufacturing. *Int Commun Heat Mass Transfer*. 2023;140:106496.

doi: 10.1016/j.icheatmasstransfer.2022.106496

126. Zhou J, Teng L, Shen Y, Jin Z. Simulation of, optimization of, and experimentation with small heat pipes produced using selective laser melting technology. *Materials*. 2023;16(21):6946.

127. Park YY, Bang IC. Experimental study on 3D printed heat pipes with hybrid screen–groove combined capillary wick structure. *Appl Thermal Eng*. 2023;232:121037.

doi: 10.1016/j.applthermaleng.2023.121037

128. Kamata M, Hayashi K, Watanabe N, *et al.* Thermal performance of ammonia-based thin flat loop heat pipe fabricated by additive manufacturing. *Int J Heat Mass Transfer*. 2025;236:126382.

doi: 10.1016/j.ijheatmasstransfer.2024.126382

129. Hunter LW, Brackett D, Brierley N, Yang J, Attallah MM. Assessment of trapped powder removal and inspection strategies for powder bed fusion techniques. *Int J Adv Manuf Technol*. 2020;106(9):4521-4532.

doi: 10.1007/s00170-020-04930-w

130. Esarte J, Blanco JM, Bernardini A, Sancibrián R. Performance assessment of a three-dimensional printed porous media produced by selective laser melting technology for the optimization of loop heat pipe wicks. *Appl Sci*. 2019;9(14):2905.

131. Yun M, Hsu WT, Shim DI, *et al.* Design and fabrication of heat pipes using additive manufacturing for thermal management. *Appl Thermal Eng*. 2024;236:121561.

doi: 10.1016/j.applthermaleng.2023.121561

132. Cui J, Hu Z, Xu W, Ma Y, Ling W, Zhou W. Selective laser melting manufacturing and heat transfer performance study of porous wick in loop heat pipe. *J Manuf Process*. 2024;124:1294-1305.

doi: 10.1016/j.jmapro.2024.07.017

133. Han Z, Chang C. Fabrication and thermal performance of a polymer-based flexible oscillating heat pipe via 3D printing technology. *Polymers*. 2023;15(2):414.

134. Arai T, Kawaji M. Thermal performance and flow characteristics in additive manufactured polycarbonate pulsating heat pipes with Novec 7000. *Appl Thermal Eng*. 2021;197:117273.

doi: 10.1016/j.applthermaleng.2021.117273

135. Jacob DJ. *Introduction to Atmospheric Chemistry*. New Jersey: Princeton University Press; 1999.

136. Zhao B, Hu M, Ao X, Chen N, Pei G. Radiative cooling: A review of fundamentals, materials, applications, and prospects. *Appl Energy*. 2019;236:489-513.

doi: 10.1016/j.apenergy.2018.12.018

137. Park S, Choi J, Lee J, *et al*. Gradient porous and carbon black-integrated cellulose acetate aerogel for scalable radiative cooling. *Small*. 2025;21(7):2409873.

doi: 10.1002/smll.202409873

138. Shi X, Liu C, Lin B, *et al*. 3D printed cellulose nanofiber/silica nanoparticle scaffolds for daytime radiative cooling. *Addit Manuf*. 2024;92:104392.

doi: 10.1016/j.addma.2024.104392

139. Zhou K, Li W, Patel BB, *et al*. Three-dimensional printable nanoporous polymer matrix composites for daytime radiative cooling. *Nano Lett*. 2021;21(3):1493-1499.

doi: 10.1021/acs.nanolett.0c04810

140. Park SJ, Seo SB, Shim J, *et al*. Three-dimensionally printable hollow silica nanoparticles for subambient passive cooling. *Nanophotonics*. 2024;13(5):611-620.

doi: 10.1515/nanoph-2023-0603

141. Hazarika A, Deka BK, Park H, *et al*. Hierarchically designed 3-D printed porous nylon fabric-based personal thermoregulatory for radiative and directional wick-evaporative cooling. *Chem Eng J*. 2023;471:144536.

doi: 10.1016/j.cej.2023.144536

142. Hazarika A, Lee S, Park H, *et al*. 3D printed gradient porous fabric-based thermal and moisture regulating composite integrated triboelectric nanogenerator for human motion cognizance. *Nano Energy*. 2024;132:110350.

doi: 10.1016/j.nanoen.2024.110350

143. Wu WL, Tsai SY, Lo YC, *et al*. Design of a multifunctional resin-based outdoor spherical robot shell for ultrahigh visible to near-infrared transmittance and mid-infrared radiative cooling. *ACS Omega*. 2025;10(3):3080-3089.

doi: 10.1021/acsomega.4c09954

144. Zhang T, Zhang X, Zhang S, Wang L, Yu D, Wang W. 3D printing-assisted honeycomb-structured bricklike aerogels applied for infrared stealth with good thermal management. *ACS Appl Polym Mater*. 2024;6(22):13828-13840.

doi: 10.1021/acsapm.4c02747

145. Pelanconi M, Barbato M, Zavattoni S, Vignoles GL, Ortona A. Thermal design, optimization and additive manufacturing of ceramic regular structures to maximize the radiative heat transfer. *Mater Design*. 2019;163:107539.

doi: 10.1016/j.matdes.2018.107539